electronic materials

MDPI

Review

From Molecular Cages to Functional Devices: Silsesquioxane Hybrid Platforms for Next-Generation Electronic Materials

Rungthip Kunthom [1,2], Chenchira Pherkkhuntod [3], Nattaya Srirattanaprasit [3] and Masafumi Unno [4,*]

[1] Futuristic Science Research Center, School of Science, Walailak University, Nakhon Si Thammarat 80160, Thailand; rungthip.ku@mail.wu.ac.th
[2] Functional Materials and Nanotechnology Center of Excellence, Walailak University, Nakhon Si Thammarat 80160, Thailand
[3] Department of Chemistry, Faculty of Science, Mahidol University, Bangkok 10400, Thailand; chenchira.phe@gmail.com (C.P.); nattaya.srirattana@gmail.com (N.S.)
[4] Department of Chemistry and Chemical Biology, Graduate School of Science and Technology, Gunma University, Kiryu 376-8515, Japan
* Correspondence: unno@gunma-u.ac.jp

Abstract

Polyhedral oligomeric silsesquioxanes (POSS) and related silsesquioxanes provide an atomically precise platform for organic–inorganic hybrid electronics. Existing reviews mainly address synthesis, functionalisation, and application breadth; comparatively few connect molecular architecture to electronic function and benchmark the resulting devices against contemporary non-POSS records. This review is organised around that structure–property–device relationship. Each cage class—closed $T_8/T_{10}/T_{12}$ cages, open-cage and double-decker frameworks, Janus cubes, ladder polymers, and ionic or fluorinated derivatives—is paired with the electronic function it enables; reported figures of merit are compared with current field records, and unresolved contradictions, trade-offs, and manufacturing barriers are stated explicitly. Device classes surveyed include light emission (OLEDs, perovskite LEDs, quantum-dot LEDs, and white LEDs), thin-film transistors and interlayer dielectrics, organic, perovskite, and dye-sensitised photovoltaics, and emerging platforms in memory, chemosensing, flexible electronics, and thermal management. We conclude that encapsulation resins, nanocrystal surface modifiers, and low-k dielectric formulations appear among the most promising candidates for translation beyond laboratory-scale demonstrations. Machine-learning-guided cage design, mixed-architecture networks, and fluorine-free routes to hydrophobicity are identified as the most credible routes to closing the remaining gaps.

Keywords: silsesquioxane; POSS; hybrid electronic materials; optoelectronics; low-k dielectrics

Check for updates

Academic Editor: Giovanni De Bellis

Received: 6 September 2026
Revised: 23 September 2026
Accepted: 28 September 2026
Published: 2 October 2026

Copyright: © 2026 by the authors. Licensee MDPI, Basel, Switzerland. This article is an open access article distributed under the terms and conditions of the Creative Commons Attribution (CC BY) license.

1. Introduction

Two trends have reshaped the requirements placed on electronic materials over the past decade: the continued scaling of solid-state electronics and the emergence of flexible, printable, and body-conformable systems. A functional layer must now cure below the softening point of plastic, survive thousands of mechanical strain cycles, resist photobleaching, and remain dispersible in the same solvent stream as the surrounding device stack [1]. Organic–inorganic hybrid materials offer a plausible reconciliation of these otherwise competing constraints, marrying the low-temperature processability of polymers to the mechanical and dielectric robustness of oxide networks [2]. Within that hybrid landscape, polyhedral oligomeric silsesquiox-

anes (POSS) and the wider silsesquioxane family occupy a distinctive niche as an atomically precise nanoscale platform for next-generation electronic materials [3,4].

Written as $(RSiO_{1.5})_n$ with n = 8, 10, 12, or 14, the empirical formula conveys only the connectivity of the cage. The interest lies in the fact that a monodisperse silicon–oxygen scaffold approximately 0.5–1 nm in diameter carries multiple vertex substituents whose chemistry and geometry can be varied independently (Figure 1) [1,5]. This combinatorial freedom lets a single cage act simultaneously as an inorganic core that geometrically isolates chromophores, a rigid nanospacer that dictates local film architecture, and a versatile coupling partner for click, hydrosilylation, and Pd-catalysed reactions [6–8]. Contributions from the groups of Laine [9,10], Chujo [11], Sellinger [12], Kuo [13], Marciniec [14,15], Rogach [16], and Ervithayasuporn [17], among others, have expanded the accessible chemistry far beyond the historical octahydridosilsesquioxane ($H_8Si_8O_{12}$) cube, giving device engineers a library of architectures with quantitatively different property profiles.

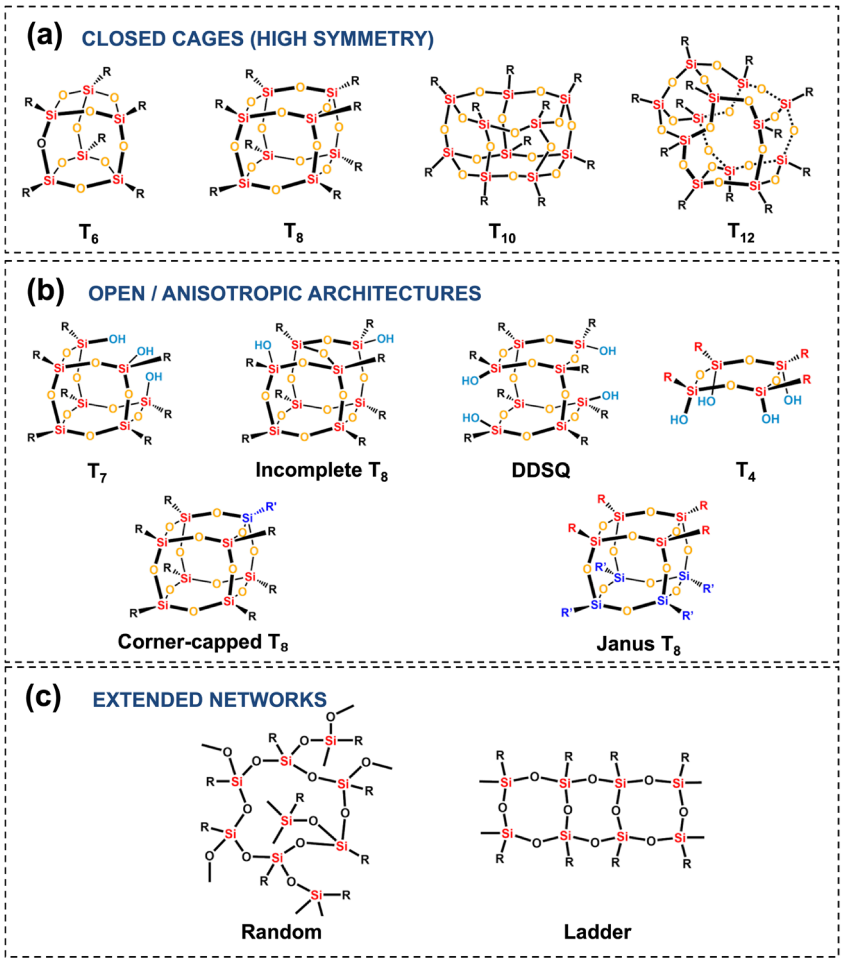


Figure 1. Structural diversity of silsesquioxane architectures relevant to electronic materials. (**a**) Representative closed-cage silsesquioxanes with highly symmetric T_n frameworks. (**b**) Structurally modified and anisotropic silsesquioxane architectures. (**c**) Extended silsesquioxane architectures represented by random and ladder-type networks.

These molecular attributes translate into measurable device-level consequences across the electronics landscape. The rigid cage suppresses chromophore aggregation and concentration quenching in organic light-emitting diodes (OLEDs) and perovskite light-emitting diodes (PeLEDs) while raising the glass-transition temperature of emissive films (Section 4) [12,13,16]; ladder polysilsesquioxane gate dielectrics have enabled carrier mobilities of approximately 0.53 $cm^2\ V^{-1}\ s^{-1}$ in pentacene organic field-effect transistors

(OFETs) and 1.2 cm^2 V^{-1} s^{-1} in solution-processed indium gallium zinc oxide (IGZO) transistors, and bifunctional POSS dielectrics allow pentacene transistors to operate at 4 V with a room-temperature ultraviolet (UV)-cured dielectric compatible with plastic substrates (Section 5) [18–20]; amine-terminated POSS passivates undercoordinated Pb^{2+} at perovskite grain boundaries, improving efficiency and environmental stability (Section 6) [21,22]; and memory, sensing, and stretchable-electronics applications complete the picture (Section 7) [23,24]. A single question threads through the treatment that follows and is largely absent from previous POSS reviews: how does the best POSS-based device compare with the best contemporary device that does not use POSS?

The POSS literature is dominated by pairwise comparisons against POSS-free controls within a single laboratory—a legitimate but insufficient benchmark, because such comparisons do not reveal whether the improvement brings the device to, or above, the current field record. As a result, headline achievements such as PeLED encapsulation, perovskite solar cell (PSC) passivation, and hybrid LED-package resins coexist in the literature with less critically assessed reports whose gains, though real, leave the device below the non-POSS state of the art. To structure the discussion accordingly, three editorial choices are made. Each device section (Sections 4–7) closes with a candid appraisal of conflicting reports and unresolved trade-offs; Section 2.4 provides an explicit structure–property–device design map that anchors every cage class to its natural electronic role; and the outlook in Section 8 shifts attention from laboratory metrics to the practical determinants of scale-up—foundry compatibility, roll-to-roll ink chemistry, and regulatory constraints on fluorinated compounds.

Table 1 positions the present review alongside representative earlier POSS reviews and identifies where each contribution differs. Prior surveys have been either exhaustive but chemistry-centric (Cordes, Lickiss, and Rataboul, 2010 [1]; Laine and Roll, 2011 [9]), targeted at a single device family (Tunstall-Garcia et al., on optics, 2021 [7]), or dedicated to synthesis (Li et al., on click chemistry, 2017 [8]). Each of these surveys emphasises a specific material class, property set, or application domain rather than integrating molecular architecture, structure–property relationships, device-level performance, and deployment considerations across multiple electronic technologies. The present review therefore organises silsesquioxane-based electronic materials along the pathway from molecular architecture to functional property, device role, and measurable performance, while addressing limitations, benchmarking difficulties, and opportunities for translation.

Table 1. Comparison of the scope and emphasis of representative reviews on POSS and silsesquioxane-based materials.

Prior Review	Year	Primary Focus	Chief Limitation from a Device Perspective	Distinctive Contribution
Cordes, Lickiss & Rataboul [1]	2010	Chemistry of cubic POSS	Foundational chemistry; limited device emphasis	Comprehensive treatment of cubic POSS synthesis, structure, and reactivity
Laine & Roll [9]	2011	Polyhedral phenylsilsesquioxanes	Primarily chemistry and materials	Detailed structure–reactivity relationships of phenylsilsesquioxanes
Tanaka & Chujo [11]	2012	Functional POSS materials and molecular design	Optical and functional materials; limited cross-device analysis	Molecular design strategies for functional POSS materials
Ayandele et al. [25]	2012	POSS-containing polymer nanocomposites	Includes semiconducting applications; composite-focused	Broad overview of polymer/POSS architectures and properties

Table 1. *Cont.*

Prior Review	Year	Primary Focus	Chief Limitation from a Device Perspective	Distinctive Contribution
Du & Liu [4]	2020	Cage-like silsesquioxane hybrid materials	Broad applications; limited device-level benchmarking	Structural diversity, functionalisation, and hybrid-material applications
Tunstall-Garcia et al. [7]	2021	Optical and photonic applications of POSS	Strong photonic and optoelectronic coverage	Comprehensive review of POSS in luminescence, sensing, and optoelectronics
Ding et al. [24]	2022	Fluorescent POSS hybrid materials for sensing	Primarily sensing and photonic applications	Design strategies for POSS-based fluorescent sensors
Kim, Park & Kwon [26]	2024	Ladder polysilsesquioxanes	Includes electronics and energy-related applications	Recent advances in ladder polysilsesquioxane (LPSQ) synthesis, properties, and applications
Moein & Kebritchi [5]	2023	POSS structure, properties, and applications	Broad; limited quantitative device benchmarking	Updated structure–property perspective
This review	2026	Structure–property–device relationships across electronic applications	Cross-device quantitative benchmarking and critical comparison	Links molecular architecture to device function, performance metrics, limitations, and practical deployment considerations

2. Structural Chemistry: Cage Families Relevant to Devices

The survey below is restricted to structural motifs whose properties have consequences for device behaviour; readers seeking synthetic detail are referred to the existing chemistry reviews [1,4,9,26]. The emphasis here is on the relationship between molecular architecture and electronic function rather than on synthetic methodology. The principal silsesquioxane architectures discussed throughout this review are summarised in Table 2, which classifies each structural family according to its symmetry, characteristic structural features, and predominant roles in electronic devices. This condensed overview provides a structural framework for the subsequent discussion of structure–property–device relationships.

Table 2. Structural classification of silsesquioxane architectures deployed in electronic devices. For each family, the empirical formula, distinguishing structural feature, and prevailing electronic role are indicated.

Architecture	General Formula	Distinctive Property	Dominant Electronic Role
T_8 closed cage	$(RSiO_{1.5})_8$	Monodisperse, 8 identical arms	OLED host, dielectric filler
T_{10}/T_{12} cage	$(RSiO_{1.5})_{10,12}$	Higher functionality density	Photoresists, electrolytes
Open-cage trisilanol	$R_7Si_7O_9(OH)_3$	3 reactive Si–OH vertices	Corner-capping precursor
Mono-substituted T_8	R_7R'-T_8	1 unique arm and 7 spectators	Polymerisable comonomer
Double-decker (DDSQ)	$Ph_8Si_8O_{10}(OH)_4$	Two tetraphenyl faces	OLED host, dielectric resin
Janus T_8 cube	$R_4R'_4$-T_8	Two distinct faces	Asymmetric interface materials

Table 2. *Cont.*

Architecture	General Formula	Distinctive Property	Dominant Electronic Role
Ladder LPSQ	$(RSiO_{1.5})_n$ ribbon	Ordered nanoscale texture	Flexible display hard coat
Mesoporous MSQ	$(MeSiO_{1.5})_n$	Porogen-templated voids (lower k)	Low-k interlayer dielectric (ILD), $k \approx 2.0$
Ionic POSS	T_8 + imidazolium/NR_3^+	Tunable ionic conductivity	Quasi-solid electrolyte
Fluorinated POSS	T_8 with C_6F_{13} arms	Surface energy < 12 mN m^{-1}	Encapsulant, antifouling

2.1. Closed Cages: T_8, T_{10}, T_{12}

Assembly of $RSiO_{1.5}$ units—each silicon engaging three Si–O–Si linkages—yields a graded family of closed polyhedra. Among them, the fully condensed T_8 cube attracts the most attention in electronic-materials work: it is a highly symmetric cubic framework of eight silicon vertices with a body-diagonal Si···Si separation of about 0.54 nm, and its eight equivalent arms give hybrids of predictable stoichiometry and geometry [1,5]. In practical materials, corner substitution frequently lowers the molecular symmetry well below the idealised O_h description. Higher homologues—T_{10} (D_{5h}), T_{12} (D_{2d}), and the recently isolated T_{14} (D_{3h}) cage [27]—offer greater arm density and marginally larger internal free volume; expressed in device terms, this translates into denser functional loading per molecule and modestly greater porosity in derived dielectric films. The distribution of T_8, T_{10}, and T_{12} cages obtained during silsesquioxane synthesis can depend strongly on reaction conditions, including solvent, temperature, catalyst, and counter-ion. Reproducible device performance therefore requires either isolation of the desired cage fraction or explicit characterisation of the cage-size distribution [28].

2.2. Open-Cage, Double-Decker, and Janus Architectures

Trisilanol precursors of composition $R_7Si_7O_9(OH)_3$ open a route to asymmetric R_7R'-T_8 species through selective corner capping—the standard entry to mono-vinyl, mono-amine, and mono-thiol POSS building blocks used as macromonomers or surface anchors [6,14]. Double-decker silsesquioxanes (DDSQ, $Ph_8Si_8O_{10}(OH)_4$) present two chemically inequivalent faces that serve as spatially addressable functionalisation sites. This anisotropy allows the separation and orientation of appended chromophores to be controlled, limiting intermolecular aggregation while preserving pathways for charge or energy transfer—a distinction that matters for emissive layers, where uncontrolled intermolecular contact suppresses solid-state photoluminescence. The DDSQ scaffold was introduced by Yoshida and co-workers [29], and its Janus character has since been used to display BODIPY and carbazole emitters at fixed inter-chromophore separations [30]. The last five years have brought several new members to the family: DDSQ derivatives accessed from difluorosilane coupling partners [31], butterfly- and basket-topology cages that combine rigid and flexible arms [32,33], tricyclic 12-8-12 laddersiloxanes [34], and tetrafunctional DDSQ scaffolds amenable to four-arm polymerisation [35]. Complementing these, Oguri, Egawa, Takeda, and Unno reported in 2016 the first Janus T_8 cube bearing two different sets of silicon-bound substituents, confirmed crystallographically [36]; a two-faced octasilsesquioxane in which Janus character arises only at the distal termini of otherwise identical arms was described independently in the same year [37]; subsequent molecular modelling has rationalised the synthesis of both T_8- and DDSQ-based Janus architectures [38]. The two anisotropic faces of the T_8 Janus cube invite

investigation as asymmetric dielectric interlayers and as monomers for orientation-controlled nanocube assemblies.

2.3. Ladder, Random, and Mesoporous Silsesquioxanes

Extending polymerisation past the discrete-cage regime affords ladder polysilsesquioxanes (LPSQ), whose double-stranded Si–O–Si backbone and regularly spaced pendant groups yield ordered nanoscale texture and mechanical hardness that outperform POSS-blended analogues in the demanding flexible-display cover application [26]. Random and mesoporous methylsilsesquioxane (MSQ) networks, in contrast, are typically produced by the porogen-templated sol–gel condensation of methyltrimethoxysilane; the resulting interlayer-dielectric (ILD) films exhibit dielectric constants down to 1.8, obtained at the cost of some modulus [39]. Cage-templated porosity is attractive because the void size is defined at the molecular level rather than by a sacrificial porogen. This advantage is conditional, however, on the cages remaining molecularly dispersed. POSS units have a pronounced tendency to self-associate, and above a system-dependent loading threshold—typically a few weight percent for physically blended cages and higher for covalently tethered or main-chain (bifunctional) cages—they segregate into crystalline or amorphous aggregates and micro-domains tens of nanometres in size, as documented by scanning electron microscopy (SEM) and X-ray diffraction (XRD) for POSS-modified polyurethanes and polyimides [6]. Such macroscopic phase separation creates uneven micro-domains and filler–matrix interfaces that compromise the structural integrity of the host polymer and introduces interfacial polarisation, moisture uptake, and voids that can raise, rather than lower, the localised dielectric loss. The idealised picture of an isolated sub-nanometre cage therefore only applies within the miscible regime, and the phase behaviour of a formulation should be verified at the loading actually used before the molecular free-volume argument is invoked.

2.4. Property Toolbox and Design Map

Four material properties account for most of the practical value of POSS in electronics. Thermally, cage-based hybrids routinely retain their integrity beyond 400 °C (5% mass-loss temperature, $T_{d5\%} > 400$ °C) and generate char yields above 50 wt% under inert atmosphere [40,41]. Their electrical response reflects intrinsic sub-nanometre free volume, which lowers the relative permittivity of optimised silsesquioxane films to $k \approx 2.0–2.5$ while retaining a Young's modulus near 3 GPa [39,42,43]. Optically, corner-group engineering spans refractive indices (RI) from 1.40 for fluorinated cages to roughly 1.58–1.60 for phenyl-rich silsesquioxanes [44]; values above 1.7 are reached only by co-formulating with high-index TiO_2 or ZrO_2 nanoparticles, at a cost to blue-wavelength transmittance [45]. At the surface, fluorinated POSS coatings exhibit water contact angles above 150°—well into the superhydrophobic regime [46].

These attributes are not independent variables. Fluorinated substituents simultaneously reduce surface energy and refractive index; aromatic substituents raise both refractive index and permittivity in parallel; and porogen loading trades mechanical modulus for lower dielectric constant. Table 3 externalises these coupled relationships and, more importantly, maps each cage architecture to the device role in which its property profile is most decisively useful.

Table 3. Structure–property–device design map. Each POSS architectural class is paired with the material property that most decisively drives its utility and with the device role in which that property proves most valuable; a representative recent reference is provided for each entry. This mapping serves as the connective thread of Sections 4–7.

Architectural Class	Dominant Property Lever	Best-FIt Device Role	Structural Rationale	Rep. Ref.
T_8, functionalised arms	Rigid isolation of chromophores	OLED/TADF host	Sub-nm spacing breaks π-stacking and suppresses aggregation-caused quenching (ACQ)	[12,13]
Fluorinated T_8 (F-POSS)	Low surface energy, low k	Encapsulant/ gate dielectric	Hydrophobic barrier; k < 2.5 with porogen	[44,46]
DDSQ/Janus cage	Anisotropic bifacial chemistry	OFET interface, asymmetric dielectric	Bifacial chemistry tunes the contact energetics	[15,36]
Ladder LPSQ	Ordered, low-defect film	OFET/transparent hard coat	Ladder ordering gives a low trap density	[18,26]
Amine-terminated T_8	Lewis-basic passivant	PSC grain-boundary passivation	Coordinates Pb^{2+}, halide vacancies	[21,47]
Ionic POSS (imidazolium)	Room-T ionic conductivity	Quasi-solid electrolyte (DSSC, Li)	Cage disrupts crystallisation and raises the ionic conductivity	[48]
Cross-linkable POSS (methacryl/epoxy)	UV/thermal cure	Solution-processed dielectric, encapsulation	Low-T cure compatible with plastics	[25,49]
Mesoporous/ porogen MSQ	Void-templated low k	Back-end-of-line (BEOL) ILD	Sub-nm pores give k = 2.0–2.5 at a modulus of 3 GPa	[39,50]
Lanthanide-bearing POSS	Sharp f-f emission	WLED phosphor, luminescent thermometry	Rigid Si–O environment sharpens emission	[51,52]

3. Functionalisation Strategies

Turning a bare cage into a working electronic material is an exercise in attaching the right arms at the right positions. Five reaction families supply almost all current practice (Figure 2, Table 4), and each brings its own combination of scalability, isomer purity, and functional-group tolerance. Because the underlying chemistry has been reviewed at length elsewhere, we restrict the discussion below to the practical elements that govern reproducibility during device fabrication.

Platinum-catalysed hydrosilylation—typically employing the Karstedt catalyst on either Si–H or vinyl-terminated POSS—remains the workhorse strategy. Under optimised conditions, octa-functional T_8 species are obtained in >85% yield with negligible α-isomer contamination [53]; a broad palette of electronically active fragments has been installed by this route, including carbazole, anthracene, boron-dipyrromethene (BODIPY), and iridium(III) and platinum(II) phosphors for solution-processed OLED hosts [54,55]. To our knowledge, thermally activated delayed fluorescence (TADF) emitter cores have not yet been installed directly on a POSS cage. Click chemistry—copper-catalysed azide–alkyne cycloaddition (CuAAC) and UV-photoinitiated thiol–ene reactions—has made POSS functionalisation broadly accessible: octa-azido-propyl and octa-mercaptopropyl derivatives couple quantitatively with alkynes or olefins at ambient temperature [8,56], and this pair of transformations now underpins the majority of fluorescent chemosensors [24,57,58] and ionic POSS electrolytes [48,59] reported in recent years.

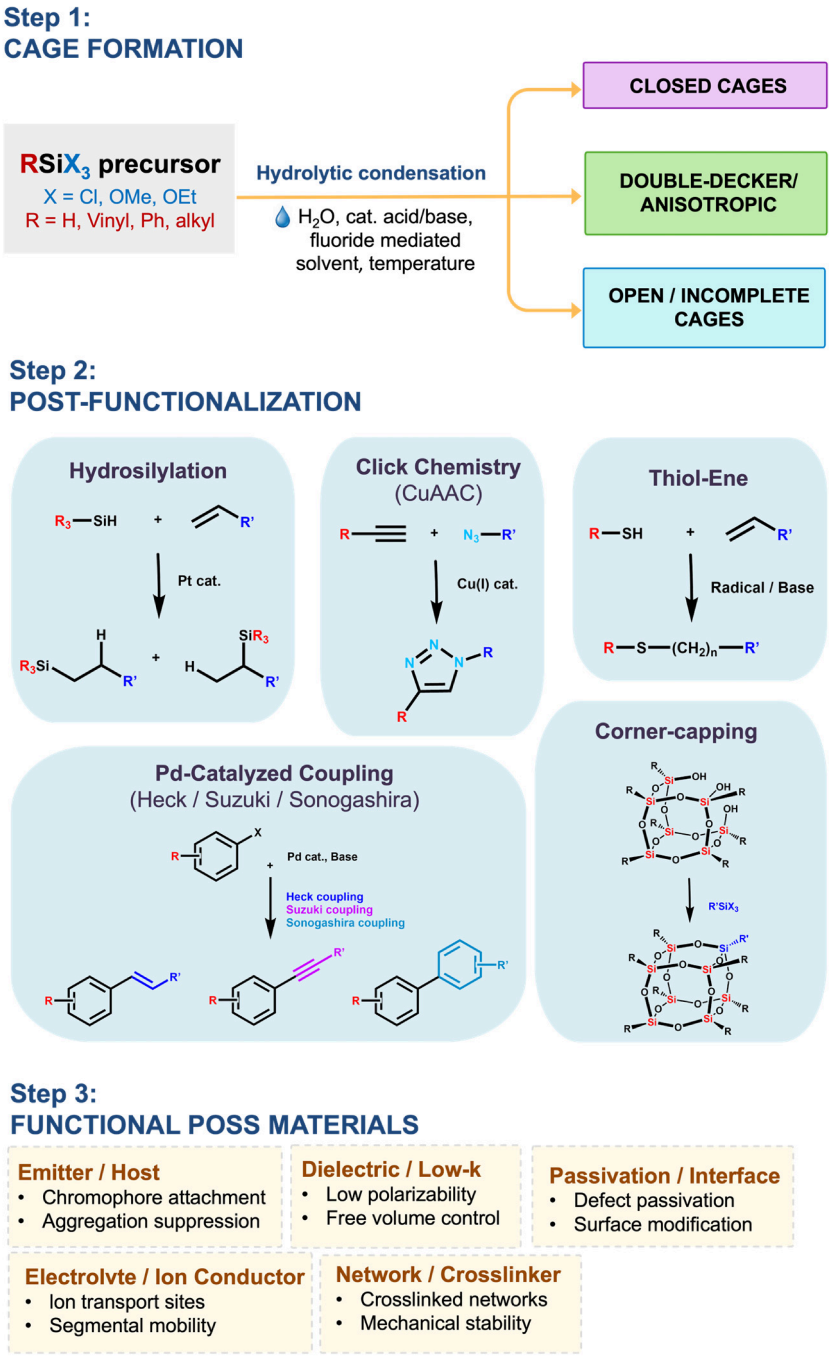


Figure 2. Synthetic pathways and post-functionalisation strategies for the preparation of functional silsesquioxane materials.

Palladium-catalysed Heck coupling on octavinyl-POSS (OVS), first exploited by Sellinger and Laine [12], continues to be the standard route to π-extended chromophore arms in OLED hosts with glass-transition temperatures (T_g) beyond 200 °C. Żak and Pietraszuk have broadened the accessible chemistry to include cross-metathesis and silylative coupling, delivering E-selective styrenic, naphthalenic, and pyrenyl arms on both T_8 and DDSQ backbones [60]. Quaternisation of octa-aminopropyl POSS by alkyl halides produces the increasingly important family of POSS-based ionic liquids (ILs) [61]; sulfonic-acid functionalisation, in a related vein, generates solid-acid platforms useful as ionic dielectric additives [17]. Polymerisable variants of POSS—carrying methacrylate, styryl, glycidyl, or norbornenyl handles—are routinely co-polymerised by radical, ring-opening metathesis polymerisation (ROMP), and step-growth chemistries; polyimide (PI)/POSS nanocom-

posites reach $k < 2.5$ while retaining $T_{d5\%} > 440$ °C, values that remain competitive with contemporary polymer dielectrics [13].

Table 4. Principal covalent functionalisation routes available for POSS derivatives. Yields represent typical values obtained under standard laboratory conditions.

Reaction	POSS Handle	Coupling Partner	Catalyst/ Conditions	Yield
Hydrosilylation	Si–H/Si-vinyl	Olefin/ hydridosilane	Pt (0) Karstedt, 60–90 °C	70–95%
CuAAC click	Si-azidopropyl	Terminal alkyne	$CuSO_4$/ascorbate, rt	>95%
Thiol–ene click	Si-thiopropyl	Vinyl, acrylate	UV/DMPA, rt	85–99%
Heck coupling	Octa-vinyl T_8 (OVS)	Aryl halide	$Pd(OAc)_2/P(o\text{-}Tol)_3$, 110 °C	60–90%
Suzuki/ Sonogashira	Octa-iodophenyl T_8	Boronic acid/ alkyne	Pd (0)/base, 80 °C	65–90%
Cross/ring metathesis	Si-vinyl	Styrenic/ norbornene	Grubbs II, rt–40 °C	80–95%
Quaternisation	Si-aminopropyl	Alkyl halide/acid	Solvent, 25–80 °C	>90%
Corner-capping	$R_7Si_7O_9(OH)_3$	$R'SiX_3$	Base, 25 °C	70–95%
Radical (co)polymerisation	Methacryl/styryl POSS	Vinyl monomer	AIBN/RAFT, 60–80 °C	Variable
Fluorosilane coupling	DDSQ + $R–SiF_2–R'$	Amines/carbonucleophiles	Base, rt	60–90%

4. Silsesquioxane Hybrids in Light-Emitting Devices

The contribution of silsesquioxanes to light-emitting devices follows from four structure–property mechanisms rather than from the chemical identity of the cage alone. First, the covalent attachment of chromophores to a rigid POSS or DDSQ framework imposes nanoscale spatial separation, reducing intermolecular aggregation and concentration-dependent quenching. Second, incorporation of the rigid Si–O framework can restrict segmental motion and increase the morphological stability of amorphous emissive films. Third, functionalised cage surfaces can modify nanocrystal interfaces through ligand coordination, surface passivation, and the suppression of interparticle ion exchange. Fourth, silsesquioxane-rich networks can act as optical and environmental barriers, where refractive-index control and reduced permeability influence light extraction and device stability, respectively. These mechanisms are exploited differently in OLEDs, PeLEDs, quantum-dot emitters, and LED encapsulation systems, as discussed in Sections 4.1–4.4.

4.1. POSS Hosts and Emitters in OLEDs: Balancing Chromophore Isolation and Charge Transport

The principal function of POSS in an emissive OLED layer is not to participate directly in charge transport but to control the spatial organisation of the electronically active components. When chromophores are covalently attached to the vertices of a rigid silsesquioxane cage, the inorganic core imposes a minimum intermolecular separation and limits the close packing that promotes aggregation-induced non-radiative decay. This geometric isolation is particularly relevant to phosphorescent and strongly π-conjugated emitters, for which high local concentrations can promote concentration quenching, excimer formation, or triplet–triplet interactions. The same structural principle extends to DDSQ derivatives, where the anisotropic scaffold provides more defined control over chromophore position and

orientation and has been used to reduce aggregation in carbazole- and BODIPY-containing systems [15,30].

A second contribution arises from the rigidity of the Si–O framework. Incorporation of POSS into molecular or polymeric hosts can restrict local segmental motion and suppress crystallisation or phase separation, thereby stabilising the amorphous morphology required for uniform OLED emission. Early solution-processed OVS-derived emissive materials demonstrated glass-transition temperatures of approximately 120–210 °C [12,62], illustrating how cage incorporation can combine molecularly defined chromophore placement with thermally robust film formation. Subsequent POSS-containing phosphorescent systems achieved external quantum efficiencies (EQEs) approaching 8–10% [54,55], while POSS-containing copolymer architectures showed improved device efficiency relative to corresponding POSS-free controls [63]. These results support the use of the cage primarily as a morphological and spatial-control element rather than as an intrinsically superior emissive unit.

Recent molecular emitters further illustrate this distinction. The POSS-MFPy device exhibited deep-blue electroluminescence at approximately 437 nm, with a maximum luminance of about 1760 cd m^{-2} and an EQE of approximately 0.19% [64]. Although this confirms the feasibility of POSS-centred deep-blue emitters, the device efficiency remains substantially below that of contemporary high-performance blue OLEDs. Assessment requires emission wavelength, EQE, current efficiency, luminance, and operational stability to be reported together.

This architecture also introduces an inherent trade-off that is more severe than a simple dilution of the electronically active groups. The silsesquioxane core is electronically insulating, and charge transport between cage-bound chromophores proceeds by hopping at a rate governed by the electronic coupling between neighbouring sites. Because that coupling decays approximately exponentially with intersite distance and is further attenuated by the intervening saturated Si–O framework, the spacing imposed by the bulky three-dimensional cage suppresses intermolecular electronic coupling far more strongly than the linear decrease in chromophore density would suggest. Increasing the POSS fraction may therefore improve morphological stability and chromophore isolation while lowering the carrier mobility disproportionately, altering charge balance, and shifting the recombination zone. The wider organosilicon OLED literature indicates how this penalty can be mitigated: in silicon-bridged aryl systems, the silicon atom interrupts π-conjugation, yet mesomeric (σ^*–π^* and through-space) interactions across the silicon centre delocalise the frontier orbitals and lower the reorganisation energy, restoring electronic coupling and yielding high electron mobility despite the insulating node [65]. Corner-group designs that deliberately build such mesomeric bridges between the chromophore and the cage—rather than fully saturated alkyl tethers—are therefore the most credible route to retaining frontier-orbital delocalisation, and hence transport, at high cage loading. The optimum POSS concentration should be regarded as a system-dependent balance between morphological stabilisation and electronic connectivity rather than as a universal loading threshold. Establishing quantitative relationships among cage loading, intermolecular spacing, carrier mobility, exciton dynamics, and OLED efficiency remains an important unresolved problem.

4.2. Perovskite LEDs: Interfacial Control, Ion-Exchange Suppression, and Environmental Protection

In perovskite light-emitting systems, POSS performs a fundamentally different function from that in molecular OLEDs. Rather than primarily separating organic chromophores, the cage acts at nanocrystal surfaces and interfaces, where its steric dimensions and functional corner groups can influence ion exchange, surface coordination, film formation, and environmental stability.

One of the clearest mechanistic advantages is suppression of interparticle halide exchange. In mixed $CsPbX_3$ nanocrystal systems, direct contact between particles can permit redistribution of halide ions and progressively alter the original emission colour. POSS encapsulation introduces a steric and chemically robust boundary around the nanocrystals, reducing interparticle contact and thereby slowing halide exchange. Huang, Rogach, and co-workers demonstrated this using POSS-coated perovskite nanocrystals, which retained their individual emission characteristics and showed improved water resistance [16]; methylsilsesquioxane aerogels have since been used for the same purpose for $CsPbBr_3$ quantum dots [66]. In this application, the principal value of POSS is therefore preservation of nanocrystal identity rather than enhancement of the intrinsic radiative transition.

POSS can also influence device performance when introduced directly into the emissive-film formulation. The improvements in brightness and EQE reported for POSS-containing green PeLEDs—peak luminance raised from 376 to 2983 cd m^{-2} and EQE from 0.02% to 0.35% [67]—are consistent with changes in nanocrystal organisation, interfacial defect density, and film morphology, but leave the device roughly two orders of magnitude in EQE below the current green PeLED state of the art, in which in situ core/shell defect suppression of the nanocrystals and charge-balance/outcoupling engineering have raised the EQE to 28.9% [68] and beyond 30% [69]. It should be stated plainly that the POSS-free control in Ref. [67] (0.02% EQE, 376 cd m^{-2}) was itself far below the performance attainable in 2016, so the eightfold gain in peak luminance and the 17-fold gain in EQE establish a mechanism rather than a competitive benchmark; measured against devices that employ modern defect-passivation strategies—core/shell nanocrystals and 2D/3D capping layers—the absolute metrics of Ref. [67] are obsolete, and the POSS-additive strategy has not yet been re-evaluated on a state-of-the-art device platform. Furthermore, these additive effects should be distinguished from the outer-shell mechanism because an additive dispersed within the film can modify several processes simultaneously, including surface passivation, particle spacing, charge injection, and percolation. Establishing which contribution dominates requires correlated measurements of film morphology, trap density, photoluminescence dynamics, and charge transport rather than device efficiency alone.

Importantly, surface encapsulation cannot correct all intrinsic perovskite defects. Its effectiveness is expected to be greatest when non-radiative losses originate predominantly from surface or interfacial states. Defects located within the perovskite lattice remain comparatively inaccessible to an external POSS shell. This distinction becomes particularly important for blue chloride-rich PeLEDs and defines a fundamental boundary between surface engineering by POSS and bulk-defect control.

4.3. Quantum-Dot LEDs and Lanthanide Phosphors

On II–VI colloidal quantum dots, mercapto- and aminopropyl-POSS serve as bidentate surface ligands, occupying both Cd and Se coordination sites on CdSe and CdSe@ZnS particles [70]. Complementary approaches based on lanthanide-bearing silsesquioxanes have opened a route to white-light emission: an octa-terpyridine T_8 chelated with Eu^{3+} exhibits white luminescence with a photoluminescence quantum yield (PLQY) of approximately 12% [51], while tetranuclear Tb/Eu silsesquioxane hybrids combine efficient Tb-to-Eu energy transfer with the additional functionality of luminescent thermometry [52]. Blending Heck-coupled octavinyl-POSS porous polymers into a polysiloxane matrix has produced hybrid white LED (WLED) phosphors with Commission Internationale de l'Éclairage (CIE) chromaticity coordinates of (0.42, 0.36), a correlated colour temperature (CCT) of approximately 2860 K, and a colour rendering index (CRI) of 90 [71].

4.4. Encapsulation and High-RI LED Packaging

For LED packaging, a thiol–ene photocurable hybrid silicone resin composed of styrene-modified mercaptopropyl-polysilsesquioxane (St-POSS-SH) and LPSQ ($n = 1.545$ at 450 nm) enabled room-temperature curing within 2 min while maintaining a self-supporting hemispherical dome, resulting in a 25.6% enhancement in light extraction efficiency for blue GaN LEDs compared with conventional flat encapsulation [72]. Phenyl-rich siloxane and silsesquioxane hybrid encapsulants reach refractive indices of 1.58–1.60 at 450 nm while retaining transmittance of 88–97%, a bounded but useful gain over conventional silicone encapsulants ($n \approx 1.41$–1.53) [45]; pushing the index above 1.7 requires high-loading TiO_2 or ZrO_2 nanocomposites, at the cost of increased blue-wavelength scattering. For comparison, the non-silsesquioxane benchmark in flexible-OLED encapsulation is a three-dyad stack of atomic-layer-deposited (ALD) Al_2O_3 and parylene C, which achieves a water-vapour transmission rate (WVTR) below 10^{-5} g m^{-2} day^{-1} [73]. These mechanisms are summarised in Figure 3.

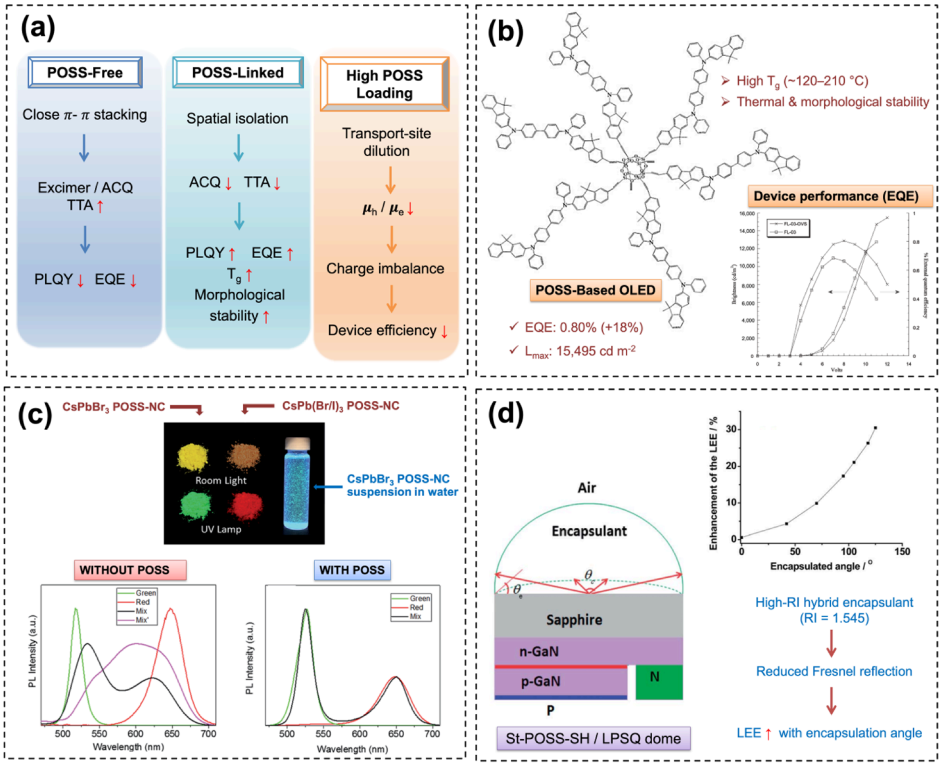


Figure 3. Mechanistic roles of silsesquioxane hybrids in light-emitting materials and devices. (**a**) Conceptual relationship between POSS incorporation, chromophore isolation, aggregation-caused quenching (ACQ), triplet–triplet annihilation (TTA), charge transport, and device efficiency. (**b**) Representative POSS-based hole-transport material and OLED performance. (**c**) POSS-coated $CsPbX_3$ nanocrystals showing enhanced water resistance and suppressed interparticle halide exchange. (**d**) High-refractive-index St-POSS-SH/LPSQ encapsulation of GaN LEDs. In (**a**) and (**d**), vertical arrows (↓) between boxes indicate the cause–effect sequence, and red arrows (↑/↓) beside a quantity denote an increase or decrease, respectively. Panel (**b**) is adapted with permission from Ref. [12], Copyright 2005 The Royal Society of Chemistry; panel (**c**) is adapted from Ref. [16] under the Creative Commons Attribution 3.0 Unported License (CC BY 3.0); panel (**d**) is adapted with permission from Ref. [72], Copyright 2014 The Royal Society of Chemistry.

4.5. Critical Assessment: Strengths, Gaps, and Conflicting Reports

A pointed question is worth asking at the end of this section: which of these deployments genuinely improves on what is already possible without POSS? Two areas answer this

question. First, among reported nanocrystal encapsulation strategies, POSS-based shells are distinctive in suppressing interparticle halide exchange while also providing environmental protection; direct comparison with polymeric and inorganic shell chemistries nevertheless remains limited, because studies use different nanocrystal compositions, shell thicknesses, and exchange protocols. Second, LED-package encapsulants formulated as POSS–siloxane resins combine refractive indices of 1.5–1.6, low optical absorption, and room-temperature cure within about two minutes—a combination that neither conventional silicones nor thermoset epoxies deliver [45,72].

The situation is more ambiguous for OLED emitters and hosts. External quantum efficiencies of 8–10% for solution-processed phosphorescent OLEDs on POSS hosts were competitive with the wider field between 2005 and 2010; a decade and a half later, contemporary phosphorescent OLEDs routinely exceed 25% EQE, and the best vacuum-deposited stacks now surpass 30% [74]. Two apparently conflicting narratives run through the intervening literature. Several groups report that POSS loading raises T_g with no penalty in charge transport, drive voltage, or operational lifetime up to roughly 40 vol%; others find that at higher loadings, the insulating cage lowers hole mobility and shifts the recombination zone, eroding the expected efficiency gain [63]. An analogous morphology–transport trade-off has been characterised in non-POSS hosts [75]. The optimum loading is therefore an architecture-dependent balance rather than an intrinsic property of POSS. The loading window over which morphological stabilisation outweighs transport loss has not been mapped systematically for any single emitter chemistry, and this is one of the more obvious experimental gaps in the current POSS-OLED literature. Three corner-group strategies are plausible routes to raising the mobility ceiling at high cage loading: (i) selecting π-extended arms—biphenyl, carbazole, or triazine—whose orbital orientation permits directional π–π overlap between neighbouring cages while retaining sub-nm chromophore isolation, (ii) using corner groups whose reorganisation energies are low relative to the transport level of the emissive layer, preserving polaron hopping through the POSS-rich matrix, and (iii) inserting mesomeric bridges—silicon-bridged aryl or σ*–π*-conjugated linkers—between the chromophore and the cage so that frontier-orbital delocalisation is maintained across the insulating core, as demonstrated for silicon-bridged electron-transport materials [65]. None of the three has received a systematic, architecture-by-architecture benchmark.

POSS has also been employed as a solution additive and hole-blocking layer in $CsPbBr_3$ nanocrystal LEDs, where it improves film morphology and raises peak luminance about eightfold (376 to 2983 cd m^{-2}) relative to the control device [67]. The comparison is, however, against a severely underperforming control: contemporary green PeLEDs built on core/shell-passivated nanocrystals or 2D/3D-capped films reach 28.9–30.8% EQE with luminance in the 10^5 cd m^{-2} range [68,69], so the POSS-modified device remains uncompetitive in absolute terms and the benefit of the cage has yet to be demonstrated on such a platform. Although quantum-dot enhancement film (QDEF) technology has already been commercialised for display backlights, efficient blue PeLEDs remain one of the major challenges for full-colour perovskite display technologies, because their efficiency, spectral purity, and operational stability all lag behind those of green and red devices [76,77].

The reasons for that deficit deserve a more physicochemical treatment than is typically offered. In blue-emissive chloride-rich $CsPb(Cl,Br)_3$ and $CsPbCl_3$ compositions, non-radiative loss is dominated not by surface defects—the regime where green Br-rich and red I-rich devices sit—but by bulk chloride vacancies. Two thermodynamic and kinetic features push blue PeLEDs into a regime that POSS shells cannot easily rescue. First, first-principles calculations show that halide vacancies are the dominant donor defects across the $CsPbX_3$ and $MAPbX_3$ families, but that the chloride vacancy introduces a deep rather than a shallow level—up to roughly 1 eV below the conduction-band minimum in chloride-rich compositions—making it

an efficient non-radiative recombination centre [78]. An outer POSS shell, however dense the sub-nm cage, does not reach the bulk defect population responsible for that loss. Second, the Pb–Cl bond is more ionic and more labile than Pb–Br or Pb–I, so Cl^- ions redistribute rapidly under the electric field of a driven PeLED; amine or carboxylate corner groups typical of POSS coordinate Pb^{2+} but do not present the chemical-potential gradient needed to trap mobile Cl^-. Closing the blue-PeLED gap will therefore require either compositional strategies that lower Cl-vacancy formation energy (mixed halide/pseudohalide mixtures, additive-mediated grain growth, 2D/3D heterostructures) or a chemical species that acts as a bulk Cl^- sink—approaches lying outside what an outer POSS shell can realistically deliver. This defines a concrete boundary of the outer-shell POSS strategy in blue perovskite electroluminescence. A more promising route—which, to our knowledge, has not yet been attempted for blue PeLEDs—would deploy an ionic POSS, for example, an octaimidazolium T_8 carrying Cl^- or pseudohalide (SCN^-, BF_4^-, or PF_6^-) counter-ions, as a bulk additive that partitions into the perovskite film during growth and fills the chloride vacancies directly. The precedent for this mechanism is well established in small-molecule form: *n*-dodecylammonium thiocyanate, a nonpolar-soluble organic pseudohalide, fills chloride vacancies in $CsPb(Br,Cl)_3$ quantum dots—a mechanism confirmed by density functional theory (DFT) to remove the in-gap electron traps—and delivers spectrally stable Rec. 2020 blue electroluminescence at 6.3% EQE [79]; long-chain ammonium chlorides act analogously in quasi-2D films, where the cation suppresses the formation of new halide vacancies while Cl^- widens the gap, reaching 15.0% EQE at 468 nm [80]. Translating that chemistry onto the monodisperse POSS backbone would combine the additive functionality with the well-defined solubility, thermal stability, and stoichiometry of the cage. Representative POSS-enabled light-emitting devices are summarised in Table 5.

Table 5. Representative POSS-enabled light-emitting devices, listed together with the year of publication and a benchmark against the current field record.

Device	Year	POSS Role	Key Metric	Value	Secondary Metric	Value	Comparison	Ref.
Solution OLED	2005–07	OVS phosphor host	EQE	2.6%	T_g	120–210 °C	Historical POSS OLED; PhOLEDs now exceed 25% EQE [74]	[12,62]
Blue OLED	2026	POSS-MFPy emitter	EQE	0.19%	Luminance λ_{EL} = 437 nm	≈1760 cd m^{-2}	Deep-blue emission demonstrated	[64]
PeLED	2016	POSS shell/additive	EQE	0.35%	Luminance	2983 cd m^{-2}	vs. POSS-free control: 0.02% EQE, 376 cd m^{-2}; state-of-the-art green PeLEDs with core/shell or 2D/3D passivation: 28.9–30.8% EQE [68,69]	[67]
WLED	2022	Ter-POSS/Eu^{3+}	PLQY	12%	—	—	Lower than high-QY phosphor systems	[51]

5. Silsesquioxane Hybrids as Dielectrics and in Transistor/Memory Devices

Three interlocking cage attributes—intrinsic sub-nanometre free volume, controllable cross-link density, and a low-energy surface—make POSS a natural candidate for the dielectric stacks that underpin organic field-effect transistors, for the interlayer dielectrics of

high-frequency interconnects, and for the trap-mediated switching layers of resistive and floating-gate memories (Figure 4 and Table 6).

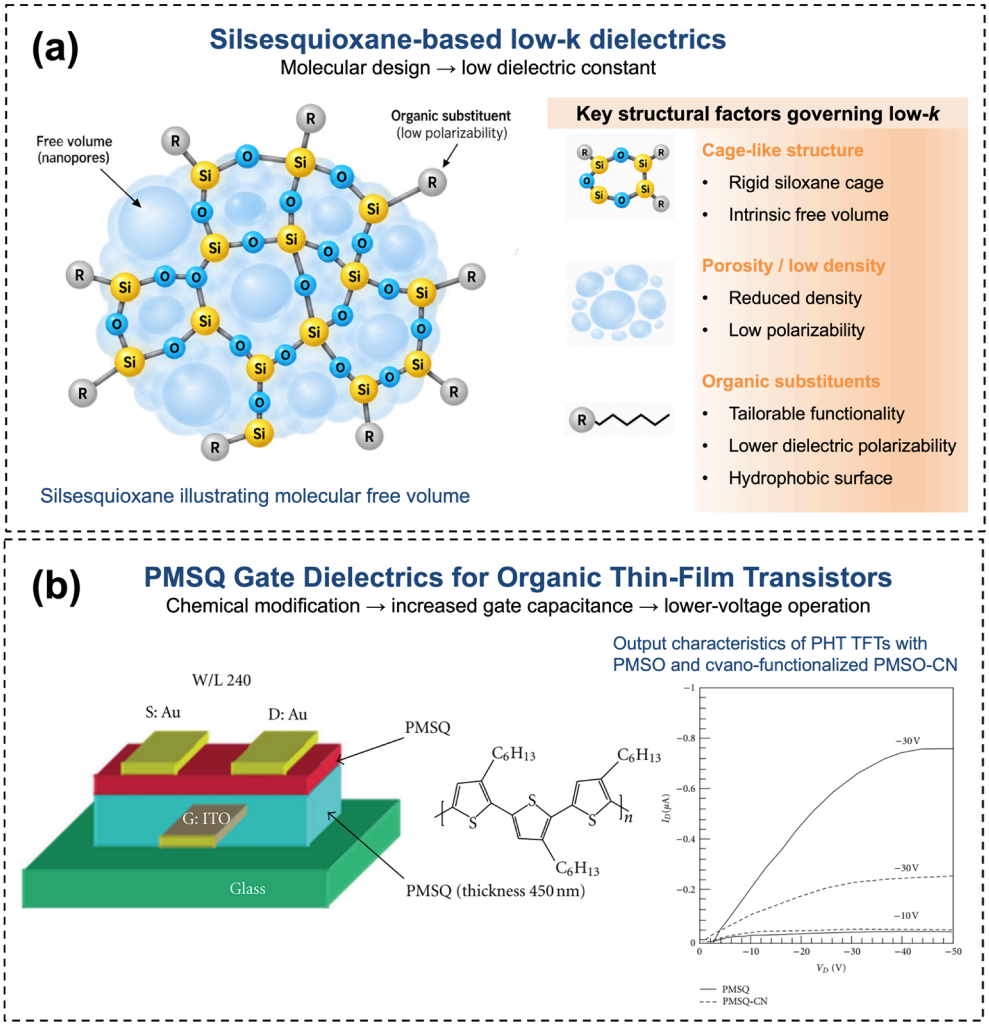


Figure 4. Structure–property relationships of silsesquioxane-based dielectric materials and organic thin-film transistors. (**a**) Molecular design principles for low-k silsesquioxane dielectrics. (**b**) Application of polymethylsilsesquioxane (PMSQ) as a solution-processable gate dielectric in a bottom-gate, top-contact organic thin-film transistor and representative output characteristics comparing PMSQ with cyano-functionalised PMSQ (PMSQ-CN). Panel (**b**) is adapted from Ref. [81] under the Creative Commons Attribution (CC BY) License.

Table 6. Representative POSS-based transistor, dielectric, and memory devices.

Device/Application	Year	Silsesquioxane Material	Role	Key Performance Metric	Reported Value	Device Condition	Benchmark Context	Ref.
Pentacene OFET	2016	Ladder PPMSQ	Gate dielectric	μ	0.53 $cm^2\ V^{-1}\ s^{-1}$	—	Compared with solution OFETs	[18]
IGZO OFET	2017	Ladder PPMSQ	Gate dielectric	μ_e	1.2 $cm^2\ V^{-1}\ s^{-1}$	—	Solution-processed IGZO	[20]
Low-voltage OFET	2021	Bifunctional POSS	Gate dielectric	C_{ox}	300 $nF\ cm^{-2}$	4 V operation (Si substrate)	Plastic-compatible process; flexible device not demonstrated	[19]

Table 6. *Cont.*

Device/Application	Year	Silsesquioxane Material	Role	Key Performance Metric	Reported Value	Device Condition	Benchmark Context	Ref.
Low-k ILD	2017	F-POSS	Interlayer dielectric	k	2.56	—	Compare with SiCOH	[82]
PI/POSS	2022	NH_2-POSS/PI	Low-k dielectric	k	2.40	1 kHz	Hybrid dielectric	[83]
Flexible RRAM	2024	NH_2-POSS	Cross-linker	Retention (flexible cell)	$>10^4$ s	switching retained after ~10^3 bending cycles	Mechanical durability; switching endurance not separately established	[23]

5.1. Low-k Interlayer Dielectrics

Spin-on formulations of POSS, hydrogen silsesquioxane (HSQ), and methylsilsesquioxane have served as low-permittivity interlayer dielectrics for the better part of two decades. Fluorinated, thermally cross-linked POSS reported by Wang and co-workers reach k = 2.56 with a dissipation factor of 3.1×10^{-3} [82]. Chemically cross-linked polyimide/POSS hybrids reach a dielectric constant of 2.40 with a dissipation factor of 0.0017 at 1 kHz and a decomposition temperature above 500 °C [83]; the earlier epoxy-POSS/polyimide systems that established the route reached k = 2.65 [84]. The Leu, Chang, and Wei experiment, in which 2.5 mol% nanoporous POSS reduced polyimide k from 3.40 to 3.09 without loss of tensile strength, remains the baseline demonstration for this route [85]. Porogen-templated POSS films span k = 1.8–2.5 depending on the loading and cure schedule [39,50].

5.2. Gate Dielectrics for OFETs

The dielectric requirements for organic transistors are more subtle: a surface roughness below 1 nm, a low interfacial trap density, and curing conditions compatible with plastic substrates. Bifunctional POSS films satisfy all three, offering a capacitance per unit area (C_{ox}) of 300 nF cm^{-2} and leakage below 10^{-6} A cm^{-2} at 2 MV cm^{-1}, and enabling pentacene OFETs that operate at 4 V with a hole mobility of up to 0.9 cm^2 V^{-1} s^{-1}; the devices were fabricated on silicon, but the UV-cured, room-temperature process is presented as compatible with plastic substrates [19]. Kang et al. showed that ladder polysilsesquioxane dielectrics support pentacene devices with $\mu = 0.53$ cm^2 V^{-1} s^{-1} and I_{on}/I_{off} exceeding 10^4, with leakage current densities below 10^{-8} A cm^{-2} at 1 MV cm^{-1} and sub-nanometre surface roughness after thermal or UV curing [18]; in the same role with solution-processed IGZO, the ladder dielectric supports an electron mobility of 1.2 cm^2 V^{-1} s^{-1} [20]. UV-cross-linked oxetane-functional POSS gives pinhole-free films that operate at low voltage on plastic [86,87].

5.3. Resistive Switching and Floating-Gate Memory

Halide-perovskite resistive memories are among the clearest beneficiaries of POSS cross-linking. Guan and co-workers reported that octa-amino-POSS grafted onto poly(acrylic acid) bridges neighbouring perovskite grains in flexible $MAPbI_3$ resistive random-access memories (RRAMs), giving retention beyond 10^4 s with resistive switching retained after roughly 10^3 bending events [23]. Spin-on HSQ RRAMs, by contrast, switch below 1 V and endure more than 10^7 switching cycles [88]; the distinguishing feature of the POSS device is therefore mechanical compliance rather than switching endurance.

5.4. Critical Assessment: How POSS Dielectrics Compare with Foundry Standards

Three tensions run through the POSS-dielectric literature. The k values of 2.0–2.5 reported for porogen-templated POSS films are attractive in isolation, but the relevant industrial benchmark is porous SiCOH at leading nodes, which combines k ≈ 2.3–2.5 with a Young's modulus of roughly 5–7 GPa [89,90]. Best-case POSS films remain near 3 GPa; modulus, not permittivity, is therefore the gating obstacle to back-end-of-line (BEOL) integration.

A specific critical knowledge gap deserves emphasis. Systematic time-dependent dielectric breakdown (TDDB), electromigration lifetime, and chemical-mechanical polishing (CMP) rate benchmarking of POSS-based ILDs against porous SiCOH under identical measurement protocols have not, to our knowledge, been published in the open literature. Because these three quantities determine whether a low-k candidate can be qualified for advanced-node insertion, their absence is itself a barrier to industrial uptake, independent of further chemical progress on the cage. A coordinated effort on these benchmarks, even for a single well-characterised POSS formulation, would do more to close the gap between laboratory demonstration and foundry qualification than another cycle of dielectric-constant optimisation. On the chemistry side, two formulation strategies are plausible routes to lift modulus without a penalty in permittivity: (i) dual cross-linking networks in which a rigid POSS-methacrylate framework is interpenetrated by a second, thermally initiated epoxy or oxetane network, so that mechanical stiffening comes from network topology rather than added polarisability; and (ii) low-loading incorporation of monodisperse silica nanoparticles (5–10 nm) into a POSS matrix, which can raise Young's modulus towards the 6 GPa target while remaining well below the percolation threshold that would raise k above 2.5. In short, POSS-based dielectrics reach k values comparable to established porous dielectrics; their remaining limitation is mechanical and reliability qualification.

The second tension concerns transistor mobility. Values reached with POSS gate dielectrics (0.5–1.2 $cm^2\ V^{-1}\ s^{-1}$) sit comfortably at the head of the solution-processed pentacene and IGZO field, but they trail crystalline silicon and single-crystal organic materials such as rubrene, which reach 10–40 $cm^2\ V^{-1}\ s^{-1}$. POSS therefore occupies the flexible, large-area, low-cost segment of the transistor landscape without pretending to challenge the high-mobility regime. In RRAMs, the distinguishing capability is mechanical: resistive switching is retained across roughly 10^3 bending cycles [23]. The reported switching endurance nonetheless remains orders of magnitude below that of spin-on HSQ cells [88], so the POSS advantage here lies in flexibility rather than cycling lifetime. The recurrent observation that heavy POSS loading raises interface roughness and trap density has yet to receive systematic architecture-by-architecture treatment.

A third tension, which the free-volume argument tends to obscure, is the loading threshold. The low-k benefit of molecularly dispersed cages is bounded by the onset of POSS aggregation and macroscopic phase separation at elevated loadings [6]: once microdomains form, the film contains filler–matrix interfaces and voids that raise interfacial polarisation and dissipation factor, lower breakdown strength, and degrade mechanical integrity, so that the dielectric loss can increase locally even while the average permittivity continues to fall. Dielectric-constant reductions reported at high POSS fractions should therefore be read together with dissipation-factor, morphology (SEM/XRD), and modulus data acquired on the same films; in the absence of such data, the loading at which the molecular-node description ceases to apply is unknown for most of the systems in Table 6.

6. Silsesquioxane Hybrids in Photovoltaics

Across all three principal families of thin-film photovoltaics—organic, perovskite, and dye-sensitised—POSS has been used as a morphology and interface modifier (Figure 5) and as

a component of encapsulation stacks that resist humidity, oxygen ingress, and thermal cycling. Representative silsesquioxane-enabled photovoltaic devices are summarised in Table 7.

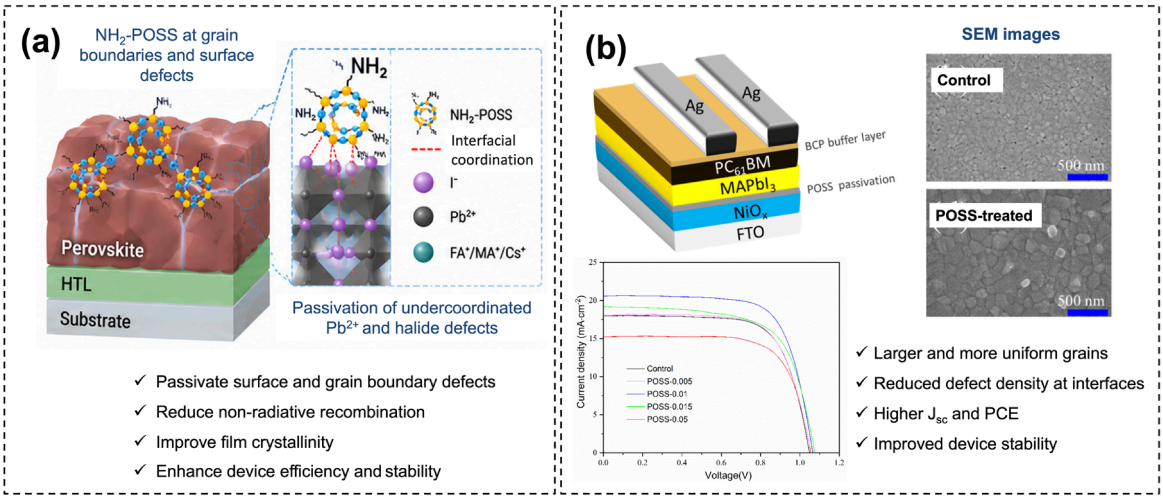


Figure 5. Interfacial engineering of perovskite solar cells using polyhedral oligomeric silsesquioxane (POSS). (**a**) Schematic representation of NH_2-POSS-mediated passivation of surface and grain-boundary defects in halide perovskites. (**b**) Representative inverted perovskite solar-cell architecture incorporating a POSS-modified NiO_x hole-transport interface. Panel (**a**) was drawn by the authors on the basis of Ref. [21]; panel (**b**) is adapted from Ref. [21] under the Creative Commons Attribution 4.0 International License (CC BY 4.0).

6.1. Organic Solar Cells

Selective functionalisation is the mechanism by which POSS operates in bulk-heterojunction organic photovoltaics. Thiol-terminated POSS anchors preferentially to poly(3-hexylthiophene) (P3HT), whereas phenyl-terminated POSS binds [6,6]-phenyl-C_{61}-butyric acid methyl ester (PCBM) through π–π interactions; the coupled effect improves the fill factor (FF) and power-conversion efficiency (PCE) of air-processed devices while retarding the thermally driven coarsening that limits their storage life [91]. Polysilsesquioxane-based hybrids have been surveyed more broadly as morphology and interface modifiers in organic photovoltaics (OPVs) [92]; quantitative operational-stability data for POSS-containing bulk-heterojunction cells, however, remain scarce. For context, binary organic solar cells (OSCs) with Y6-class acceptors reached 17.4% by 2022 [93], and single-junction organic cells now exceed 20% certified PCE [94].

6.2. Perovskite Solar Cells

Halide-perovskite photovoltaics now represent the fastest-growing application of POSS in solar technology, with the molecule occupying three distinct mechanistic roles. As a grain-boundary and surface passivant, amine-terminated POSS coordinates undercoordinated Pb^{2+} and lowers the trap-state energy level, an effect surveyed across POSS-modified perovskites [22,47]. Applied as an ultrathin overlayer on the hole-transport layer (HTL), POSS raises the short-circuit current density from 18.0 to 20.5 mA cm^{-2} and the open-circuit voltage from 1.05 to 1.07 V, lifting the efficiency from 13.3% to 15.6% [21]. As an encapsulant, however, the evidence base is thinner than the POSS literature implies: the barrier stacks credited with water-vapour transmission rates in the 10^{-5} g m^{-2} day^{-1} range are atomic-layer-deposited Al_2O_3/parylene dyads that contain no silsesquioxane [73,95], and we are not aware of a primary report of a silsesquioxane-based encapsulant being measured against that benchmark. Beyond photovoltaics, POSS has also emerged as an effective interfacial engineering material for perovskite scintillators. Functionalisation of $CsPbBr_3$ nanocrystals with aminopropylisobutyl POSS simultaneously provides surface

passivation and physical encapsulation, achieving a scintillation light yield of 23,660 photons MeV^{-1} while substantially improving radiation tolerance and environmental durability, thereby enabling high-resolution and stable X-ray imaging [96].

6.3. Dye-Sensitised Solar Cells

POSS-based ionic liquids have been a significant route to converting liquid dye-sensitised solar cell (DSSC) electrolytes into quasi-solid gels. Working with the archetypal poly(ethylene oxide) (PEO)-POSS system, Čolović et al. reported a 7% relative gain in efficiency compared with the corresponding non-additive electrolyte [59]. In a more recent development, Koymeth and co-workers demonstrated that dispersing 30 wt% of an octa-charged POSS in 1-butyl-3-methylimidazolium bis(trifluoromethanesulfonyl)imide ([BMIM][NTf_2]) pushes the room-temperature ionic conductivity of the resulting quasi-solid gel to 4 mS cm^{-1} [48]. A complementary molecular-design strategy—alkoxysilyl-anchored organic dyes, which employ a monomeric silyl anchor rather than a silsesquioxane cage—has taken metal-free organic-dye DSSCs past 12% in-house efficiency [97].

6.4. Critical Assessment: PSC PCE Gains vs. Modern Non-POSS Reference Cells

Perovskite-solar-cell reports involving POSS typically claim improvements from a baseline efficiency of 14–18% to 18–22% following POSS passivation or interlayer insertion. That improvement is real; contextualising it against the wider field is nevertheless essential. Certified single-junction PSCs now reach 27.3% [98], and none of the record-holding devices rely on POSS-based passivation. Instead, they exploit organic ammonium halides, alkylammonium salts, phenethylammonium (PEA) and phenylbutylammonium (PBA) cations, and thin 2D-perovskite capping layers. POSS thus does not currently belong to the front-of-field passivation toolbox at the highest reported efficiencies—though it does consistently improve stability metrics such as T_{80} lifetime and damp-heat survival relative to matched controls. In encapsulation, alternating ALD-grown Al_2O_3 and polymer layers achieve water-vapour transmission rates below 10^{-5} g m^{-2} day^{-1} [73]; the same design principle is increasingly applied to perovskite solar-cell encapsulation, where the moisture barrier governs long-term operational and damp-heat stability [99]. Comparable barrier data for silsesquioxane-based encapsulants have not been reported, so POSS cannot presently be ranked against this benchmark. Contradictory findings exist as to whether POSS additives accelerate or retard perovskite crystallisation; the direction of the effect appears to be governed by the corner-group chemistry (amine substituents act primarily as crystallisation modifiers, whereas alkyl arms function as hydrophobisers) [22,96]. Systematic corner-group screens would go a long way towards resolving this ambiguity.

Table 7. Representative silsesquioxane-enabled photovoltaic devices.

PV Class	Year	Silsesquioxane Role	Architecture	Key Metric	Value	Stability/Secondary Metric	Benchmark Context	Ref.
OPV	2013–16	Morphology stabiliser	P3HT/PCBM	PCE	increase vs. control	FF improved	record single-junction OSC > 20% [94]	[91]
PSC	2018	NH_2-POSS passivation	n–i–p	PCE	20.5% (control 18.1%)	Trap level 0.045 eV	vs. control/contemporary PSC	[47]
PSC	2021	POSS-modified HTL	inverted	J_{sc}	20.5 mA cm^{-2}	V_{oc} 1.07 V	vs. control	[21]
DSSC	2019	PEO-POSS IL additive	DSSC	PCE change	+7%	vs. control	relative improvement	[59]

7. Sensors, Flexible/Wearable Electronics, and Thermal Management

7.1. Fluorescent and Electrochemical Chemosensors

The treatment below is deliberately compact (representative POSS-based chemosensors and thermal-management materials are summarised in Table 8); for a comprehensive survey of the fluorophore–POSS chemosensor literature, we refer readers to the review by Ding and co-workers [24]. Rigid attachment of rhodamine, BODIPY, naphthalimide, or pyrene reporters to the POSS scaffold underpins a well-developed family of chemosensors detecting ions and explosives at nanomolar concentrations—examples include Fe^{3+}, with a limit of detection (LOD) of 7.9×10^{-8} M [100], Hg^{2+} (0.008 μM) [101], Zn^{2+}/Cu^{2+} below 200 nM [102], and picric acid via OVS-triphenylamine porous polymers with $K_{SV} > 10^5$ M^{-1} [103]. Near-infrared (NIR)-emitting silsesquioxane–thiophene porous polymers respond to iodine [104], and molecularly imprinted POSS films are beginning to address the long-standing selectivity gap in complex biological matrices [105,106]. From an electronic-device perspective, the more relevant angle is the integration of POSS-supported reporters into flexible, printable sensor arrays and electronic noses—a direction for which the platform's solution processability and low-temperature cure are well suited but which remains largely unexplored.

7.2. POSS in Flexible and Stretchable Substrates

Polyurethane (PU)/POSS composites have established themselves as the default stretchable substrate for skin-mounted and wearable electronics. In one representative example, Zhao and co-workers produced PU/POSS films exhibiting a Young's modulus of 21.8 MPa, elongation at break approaching 1000%, and water contact angles up to 121° [107]. A conductive poly(vinyl alcohol) (PVA)/phytic acid/NH_2-POSS hydrogel featuring a dense three-dimensional microporous network has demonstrated a tensile strength of 361 kPa and an elongation at break of 363%, providing an attractive combination of toughness, stretchability, and conductivity for wearable strain-sensing applications [108]. POSS has been incorporated into self-healing polymer networks—through reversible Diels–Alder linkages and dynamic disulfide bonds—to enhance mechanical robustness while preserving the reversible interactions that enable autonomous repair [109,110]; reported recovery of tensile strength is typically 70–90%.

7.3. Thermal Management and Dielectrics for Power Electronics

Incorporating epoxy-functionalised DDSQ into polybenzoxazine matrices improves their thermomechanical and dielectric behaviour. In a polysiloxane-imide-containing benzoxazine, DDSQ epoxy lowered the coefficient of thermal expansion by up to approximately 34% and raised the storage modulus by up to 183% while leaving $T_{d5\%}$ essentially unchanged (419 °C versus 410–413 °C) [111]; in a conventional polybenzoxazine, 1–4 wt% of a bifunctional DDSQ epoxy raised $T_{d5\%}$ by up to 16 °C, shifted the temperature of the maximum mass-loss rate upwards by approximately 56 °C, and lowered the dielectric constant from 3.75 to 3.45 [112]. A related DDSQ modification raises the decomposition temperature to 427 °C with a char yield above 50 wt% [113]. The reductions in dielectric constant and loss reported for DDSQ-modified benzoxazines [112] point to this resin family as a candidate for mmWave circuit boards, although the values reported so far ($k \approx 3.45$) remain above the $k < 3$ typically targeted for such substrates. On the mechanical side, POSS-modified epoxy formulations combine high glass-transition temperatures ($T_g \approx 260$ °C), percolated electrical conductivity at low nanotube loading, and measurable self-healing efficiency, illustrating the multifunctionality accessible from a single 5 wt% cage addition [114].

7.4. Critical Assessment: Sensor Selectivity, Wearable Durability, and the Limits of POSS in Thermal Management

POSS chemosensors advertise impressive detection limits—10^{-8} M for Fe^{3+} and nanomolar thresholds for Zn^{2+}/Cu^{2+} [100,102]—but those figures are almost always established against a narrow panel of competing ions. Interference from the alkali and alkaline-earth cations that dominate real samples is rarely quantified, and the cross-sensitivity data needed to convert a detection limit into an operational specification are seldom reported. A distinction between the two sub-literatures is worth drawing here. Molecularly imprinted POSS sorbents have been validated in genuinely complex matrices—fluoroquinolone extraction from milk [105] and nucleoside recovery from urine [106]—whereas the fluorescent POSS reporters that dominate the sensing literature are still characterised almost exclusively in clean aqueous or aqueous–organic media, including the more recent antibiotic platform [115]. Silsesquioxane–polyoxazoline adsorbents evaluated on spiked river-water samples, with quantification by ambient flowing-atmospheric-pressure-afterglow mass spectrometry (FAPA-MS) down to 0.05 µM [116], belong with the former group rather than the latter, and are better described as sorbents with instrumental read-out than as sensors. Transferring the matrix discipline of the former to the latter is the obvious next step, and it is a prerequisite for any of these chemistries reaching an integrated, printed sensor array.

In wearable strain sensing, the combination of high gauge factor and adequate mechanical compliance is by now well documented [107,108], but the durability metrics that determine consumer viability are not. Cyclic testing is rarely extended beyond approximately 10^3 deformation cycles, and resistance to sweat, sebum, and skin lipids—the actual failure mode for skin-mounted hydrogels and elastomers—is essentially absent from the POSS literature. Self-healing POSS networks present a related asymmetry: Diels–Alder and dynamic disulfide chemistries restore 70–90% of tensile strength [109,110], yet electrical function is almost never measured across the same healing cycle. Cubic-POSS-capped polyurethane/poly(3-hexylthiophene) films demonstrate that mechanically compliant, conductive POSS hybrids are achievable [117]; coupling that conductivity to a quantified healing protocol—recovery of both electrical conductivity and tensile strength after a defined damage event, reported together—remains an open and readily addressable target.

Thermal management deserves a more careful reading than it usually receives, because the available data are easy to over-interpret in either direction. Zhao and co-workers report that an epoxy composite filled with boron nitride nanosheets together with a glycidyl-functionalised POSS reaches a thermal conductivity of 0.397 W m^{-1} K^{-1}, approximately 115% above the unfilled resin, while simultaneously lowering the dielectric constant and dissipation factor [118]. Two points follow. First, the authors attribute the thermal enhancement to the high-aspect-ratio boron nitride phonon pathways and credit the cage with the dielectric response rather than with heat transport. The same study, however, also contains the diagnostic control: at the same 20 wt% boron nitride loading the POSS-free composite reaches 0.55 W m^{-1} K^{-1}, so that the addition of 2 wt% glycidyl-POSS lowers the thermal conductivity by roughly 28% (Ref. [118] quotes 38%, a figure calculated relative to the POSS-containing composite), an effect the authors attribute to the nanoscale voids of the cage scattering phonons and to partial POSS agglomeration that interrupts the boron nitride percolation network [118]. In this system, therefore, the two competing expectations—cage free-volume scattering phonons versus improved filler dispersion enhancing network connectivity—are resolved in favour of the former: the cage delivers the dielectric benefit at a measurable cost in heat transport, and the 115% figure quoted against neat epoxy should not be read as a contribution of POSS. Second, even the boron-nitride-only value remains an order of magnitude below the ceramic-filled thermal interface materials (TIMs) used in power-electronics packaging. The practical conclusion is unchanged from the one usually

drawn, but it should be reached for the right reason: POSS earns its place in power electronics as a low-k, low-coefficient-of-thermal-expansion (CTE), thermally stable dielectric that tolerates the thermal load—not as a bulk heat spreader, and with the expectation that the cage voids impede rather than assist phonon transport.

Table 8. Representative POSS-based chemosensors and thermal-management materials reported between 2014 and 2025.

Application	Year	POSS Material	Analyte/Function	Performance	Ref.
Fluorescent sensor	2021	Imidazolium-POSS IL	Fe^{3+}	LOD 7.9×10^{-8} M	[100]
Fluorescent sensor	2020	Selenone-POSS	Hg^{2+}	LOD 0.008 μM	[101]
Fluorescent sensor	2023	Rhodamine click POSS	Zn^{2+}/Cu^{2+}	LOD 3.0–40 nM	[102]
Explosive sensor	2014	OVS-triphenylamine polymer	Picric acid	$K_{SV} > 10^5$ M^{-1}	[103]
Iodine sensor	2023	SQ-thiophene NIR polymer	I_2 vapour/solution	High capacity, NIR emission	[104]
Antibiotic sensor	2025	SQ hybrid polymer	Tetracycline	LOD 0.05 μM; photodegradation	[115]
Pesticide adsorbent/ preconcentrator	2026	OV-SQ/poly(2-phenyl-2-oxazoline)	Pesticides in environmental water	BET surface area 460 m^2 g^{-1}; ambient FAPA-MS after adsorptive preconcentration: LOD 0.05 μM (MCPA, COOH-functionalised sorbent; 200-fold lower than direct analysis) and 0.5–1 μM (picloram, atrazine); recovery within 3% in spiked river water	[116]
Strain sensor	2020	PVA/phytic acid/NH_2-POSS	Body motion	ε 363%, σ 361 kPa	[108]
Stretchable conductor	2019	Cubic-POSS PU + doped P3HT	Wearable wires	>1 S cm^{-1} under strain	[117]
Self-healing elastomer	2018	Diels–Alder PU-POSS	Coating/skin	Crack closure and tensile recovery	[110]
TIM/packaging	2022	DDSQ-epoxy/cyanate ester	Heat dissipation	T_d 427 °C, char 51 wt%	[113]

8. Cross-Device Assessment, Manufacturing, and Outlook

8.1. Where POSS Is Most Competitive: A Cross-Device Impact Summary

Taken together, the preceding sections support an impact ranking. The contributions of POSS that are most distinctive and closest to industry are, in descending order: LED and OLED encapsulation resins, which offer an attractive combination of refractive-index control, environmental protection, and low-temperature processing; perovskite nanocrystal shells that block interparticle halide exchange; hybrid low-k interlayer dielectrics where modulus is preserved; and OFET gate dielectrics in flexible, large-area formats. Perovskite-solar-cell encapsulation is frequently listed as a POSS strength but is not yet supported by a primary silsesquioxane barrier measurement. Conversely, POSS lags the field when compared with record-holding OLED emitters (currently at >30% EQE) and PeLEDs (28.9–30.8% EQE [68,69]), with the leading passivation chemistries used in >27–certified PSCs, and as a bulk heat spreader in power-electronics packaging. Table 9 encapsulates these judgements in a single-glance form.

Table 9. Cross-device assessment of opportunities, limitations, and translation priorities for silsesquioxane- based electronic materials.

Device/Application	Primary POSS Function	Demonstrated Advantage	Main Limitation	Key Step Towards Translation
LED/OLED encapsulation	High-RI and barrier encapsulant	Improved optical extraction and environmental protection demonstrated in laboratory devices	Long-term photostability, yellowing, cost	Long-duration reliability testing and industrial packaging qualification
PeLED/QLED shell	Nanocrystal isolation and halide-exchange suppression	Strong suppression of interparticle halide exchange and improved environmental stability	Limited control of bulk defects, particularly in blue emitters; device metrics not yet benchmarked against modern core/shell- or 2D/3D-passivated PeLEDs [68,69]	Operational-lifetime testing and scalable shell processing
OLED host/emitter	Chromophore isolation and morphological stabilisation	Reduced aggregation and improved thermal/morphological stability	Exponential loss of intersite electronic coupling (charge-transport penalty) at high POSS content unless mesomeric bridges are built in [65]	Systematic loading–mobility–EQE correlation and lifetime benchmarking
PSC passivation additive	Surface/interface coordination	Reduced interfacial losses reported in selected systems	Effect is chemistry- and interface-dependent	Standardised control devices and long-term stability validation
PSC encapsulation	Moisture/oxygen barrier	Concept plausible, but the reported low-WVTR stacks are ALD inorganic/organic dyads, not silsesquioxane	No primary silsesquioxane barrier measurement; ALD cost and scale-up	Large-area and accelerated-ageing validation
Flexible OFET dielectric	Low-temperature-processable dielectric	Suitable capacitance and flexible device operation	Mobility and reliability depend strongly on formulation	Bias-stress, bending-cycle and large-area uniformity testing
Low-k ILD	Sub-nanometre free volume/low polarisability	Low dielectric constants demonstrated	Mechanical integrity and reliability; aggregation/phase separation and rising dielectric loss above the POSS loading threshold [6]	TDDB, electromigration, CMP and integration testing
Flexible RRAM	Structural/interface modification	Resistive switching demonstrated	Device-to-device and cycle-to-cycle variability	Statistical endurance and array-level validation
Chemical sensors	Rigid fluorophore scaffold	High sensitivity/selectivity in model systems	Matrix interference and fouling	Validation in real samples and long-term calibration
Wearable materials	Hybrid cross-linking/mechanical reinforcement	Flexibility and functional stability demonstrated	Sweat, lipid and cyclic durability	Extended mechanical/environmental testing
Thermal-management materials	Low-CTE hybrid dielectric	Dimensional stability and dielectric functionality	Thermal conductivity below ceramic-rich TIMs	Thermal cycling and package-level testing

8.2. Manufacturing Considerations: From Beaker to Product

Four industrial obstacles recur across the POSS applications examined above. The first is the cost and isomer purity of asymmetric POSS cages at the kilogram scale. The second is compatibility with roll-to-roll deposition, particularly ink rheology, curing kinetics, and edge-bead management. The third is foundry integration, which demands CMP-tolerant, plasma-etch-tolerant, low-CTE films that qualify against established benchmark suites. The fourth is regulatory pressure on fluorinated POSS derivatives.

On the ink side, the low crystallisation tendency of POSS is a genuine asset for smooth spin-coated and inkjet-printed films, but its favourable solubility in aromatic solvents such as toluene and chlorobenzene sits awkwardly with the transition to green-solvent inks already underway in OPV and PSC pilot production. Hansen-solubility-parameter mapping, which identifies the ester and alcohol solvents that dissolve a given cage substitution [119], and work on aqueous POSS dispersions [120] are therefore priority developments. In roll-to-roll UV-cure POSS-acrylate resins, cure exotherm and shrinkage continue to necessitate careful acrylate/POSS stoichiometry.

The foundry-integration story turns on a small set of missing benchmark data. Chief among them are (i) time-dependent dielectric breakdown statistics under operating field, (ii) electromigration resistance of embedded copper interconnects, and (iii) CMP polish-rate matching to adjacent SiCOH. These are the benchmarks of the International Technology Roadmap for Semiconductors (ITRS) and its successor, the International Roadmap for Devices and Systems (IRDS), that academic publications rarely include [121]. On the lithography front, silsesquioxane e-beam resists have delivered 14 nm features with a line-edge roughness of 1.3 nm [122,123], although extreme-ultraviolet (EUV) printability of HSQ at 16 nm dense pitch still shows a line-edge roughness near 6.4 nm at high dose [124]; etch selectivity to underlying SiO_2 remains below that of the incumbent acrylate resist chemistries.

8.3. Sustainability and Fluorine-Free Hydrophobicity

Fluorinated POSS can achieve surface energies of approximately 12 mN m^{-1} or below, substantially lower than those of many hydrocarbon- and siloxane-based surfaces [46], but tightening regulatory pressure on per- and polyfluoroalkyl substances (PFAS) is beginning to compromise its commercial viability. The point is not incidental: under the structure-based definition adopted by the Organisation for Economic Co-operation and Development (OECD) in 2021—any substance containing at least one fully fluorinated methyl ($-CF_3$) or methylene ($-CF_2-$) carbon bearing no H, Cl, Br, or I—a C_6F_{13}- or 1H,1H,2H,2H-perfluorooctyl-substituted cage is unambiguously a PFAS [125]. The same definition underpins the universal PFAS restriction proposal submitted to the European Chemicals Agency (ECHA) in 2023 by five European national authorities, which explicitly brings side-chain fluorinated substances within scope on the grounds that they degrade to non-polymeric perfluoroalkyl acids [126]. F-POSS is therefore not merely adjacent to the regulatory debate; it sits inside the restricted class as defined. This has pushed the community towards fluorine-free alternatives: long-chain alkyl, siloxy-rich, and hierarchically textured POSS coatings that recover much of the hydrophobic performance without the environmental liability [127,128]. Three concrete non-fluorinated strategies have gained traction in the last two years and deserve mention. First, fluorine-free alkyl- and siloxy-functionalised silsesquioxane coatings on cotton reach water contact angles of 146–151°, within a few degrees of fluorinated controls [128,129]. Second, POSS–siloxane hybrids in which the fluorinated arm is replaced by siloxy-functional silanes achieve contact angles above 145° and retain water repellency over 100 abrasion cycles [128]. Third, surface texturing offers a route that is independent of arm chemistry altogether. It is well established in the broader coatings literature that dual-scale, hierarchical roughness stabilises the Cassie–Baxter wetting state

and can push intrinsically hydrophobic—but not superhydrophobic—polymer surfaces past 150°, with roughness supplied either by dispersed silica nanoparticles or by templated micro/nano structuring [127]. The fluorine-free silsesquioxane coatings discussed above already exploit this effect implicitly, since the 146–151° contact angles reported on cotton arise from the combination of low-surface-energy arms with the intrinsic hierarchical texture of the fabric substrate rather than from surface chemistry alone [128,129]. What has not been done, to our knowledge, is a controlled test of the same principle on a planar, unmodified alkyl-POSS film—deliberately roughened by nanoparticle loading or by phase separation during cure—where the chemical and topographical contributions could be separated. That experiment would establish how much of the fluorine-free performance gap is recoverable by topography alone, and it is a prerequisite for extending fluorine-free silsesquioxane coatings from textiles to the planar encapsulant and wearable-substrate geometries that matter for electronics.

8.4. AI-Guided Design, High-Throughput Screening, and Closed-Loop Synthesis

The combinatorial size of the POSS design space—cage symmetry × vertex functional group × counter-ion × surrounding polymer matrix—is exactly the regime in which machine-learning (ML) surrogates and Bayesian optimisation prove most valuable. Computational work on POSS remains largely confined to molecular simulation, electronic-structure calculation, and solubility-parameter estimation [119]. To our knowledge, no generalisable machine-learning property-prediction model for arbitrary POSS derivatives has been reported, although inverse-design workflows are now established for polymers and inorganic materials more broadly [130]. Closed-loop platforms that couple ML-based property prediction to robotic synthesis are gaining momentum in the wider materials-informatics community [131]. POSS is a particularly favourable target for this workflow, because its cage geometry is essentially invariant across arm substitutions—giving surrogate models a stable structural anchor against which arm-level chemistry can be varied systematically.

Two directions stand out. Generative models can, in principle, propose corner-group combinations that jointly satisfy multiple targets—for instance, $k < 2.5$, WVTR below 10^{-5} g m^{-2} day^{-1}, T_g above 220 °C, and no fluorinated arms—dramatically shrinking the synthetic effort needed to hit a specification. Complementary to this, uncertainty-aware active learning systematically identifies the small number of unseen cages whose measurements would most improve the surrogate model, a workflow already demonstrated for organic semiconductors and now being ported to hybrid materials. Given the structural rigidity of POSS, the first ML-designed POSS dielectrics and encapsulants may plausibly appear within a few years; no such demonstration has yet been reported for POSS specifically, and the projection rests on analogy with adjacent hybrid-material classes.

8.5. Frontier Directions: Mixed-Cage Networks, Bioresorbable POSS, and Quantum/Neuromorphic Platforms

Networks that interleave two cage architectures—T_8 with T_{10}, or T_8 with DDSQ—at controlled stoichiometry access bimodal pore distributions and dielectric or mechanical responses that neither parent cage exhibits alone. Bioresorbable electronics represent another conceptually interesting frontier. Although POSS-based materials have been explored extensively in biomedical systems [132], their translation into transient electronic devices has not yet been established. Bioresorbable silicon electronics demonstrate the feasibility of transient implantable devices more broadly [133], suggesting—rather than demonstrating—a potential future opportunity for appropriately designed degradable silsesquioxane hybrids. Lanthanide-silsesquioxane cages behave as field-induced single-molecule magnets and as bifunctional magneto-luminescent materials—a class of interest for molecular magnetic

memory and luminescent thermometry [52,134]. Given the importance of dielectric/interface engineering in emerging 2D electronics [135–137], integrating molecularly tunable silsesquioxane dielectrics with two-dimensional semiconductors is a further, as yet unexplored, opportunity. We flag explicitly that the quantum, neuromorphic, and bioresorbable directions currently rest on a small number of proof-of-principle papers rather than an established literature; the discussion here should therefore be read as an orientation to plausible research directions, not as an assessment of technologies already competitive with non-POSS alternatives.

8.6. Standardised Reporting: A Concrete Checklist

Performance metrics are still frequently reported without the accompanying details of cage composition, cure conditions, and full device architecture. To make the recommendation actionable, we propose the following minimum reporting set for future POSS-electronics studies, modelled in part on established stability-reporting frameworks for organic and perovskite photovoltaics [138,139]: (i) POSS cage identity—isomeric purity by gel permeation chromatography (GPC) and/or ^{29}Si nuclear magnetic resonance (NMR) spectroscopy ($T_8/T_{10}/T_{12}$ ratio), polydispersity index, and, for functionalised cages, the average number and identity of arms per cage; (ii) film processing—solvent, solids loading, spin/inkjet parameters, cure temperature, time, and atmosphere; (iii) device architecture—substrate, all electrode materials with work functions, all layer thicknesses measured (not nominal), and any interfacial treatments; (iv) measurement conditions—illumination spectrum and intensity for photovoltaic devices, sweep rate and direction for J–V curves, humidity and temperature during measurement, and storage conditions between fabrication and testing; (v) benchmarking—the strongest available non-POSS reference of the same class prepared on the same substrate in the same laboratory, together with numerical rather than qualitative comparison; and (vi) stability—T_{80}/T_{90} metric under a specified stress protocol. For each of these categories, we recommend explicit reference to established industry standards wherever they exist: ISOS-D-1/D-3 (ambient dark storage/damp-heat), defined for organic PV [138] and adapted for perovskite devices [139]; JEDEC JESD22-A101 (85 °C, 85% relative humidity, RH) for encapsulated devices [140]; American Society for Testing and Materials (ASTM) D3359 for barrier-coating adhesion [141]; ISO 4287 for surface-roughness metrology [142]; IEC 62631-3 for volume/surface resistivity of dielectrics [143,144]; IEC 60112 for comparative tracking index [145]; and IEC 61215 for module-level accelerated ageing [146]. Adoption of this checklist would improve reproducibility and permit the cross-group meta-analyses the field currently lacks.

9. Conclusions

POSS should be regarded not as a universal replacement for established electronic materials, but as a molecularly defined platform that can provide distinct advantages in selected applications. Its most compelling opportunities arise when cage-scale architecture, functional-group control, and hybrid processing collectively address limitations that are difficult to resolve through a single conventional material. At the same time, the available literature indicates that substantial gaps remain in charge transport, long-term reliability, large-scale processing, cost, and direct comparison with state-of-the-art device materials. In arenas where record-breaking device performance is set by different chemistries, POSS competes less effectively. The field should concentrate effort on the problems that POSS is uniquely positioned to solve rather than on further pairwise improvements over ad hoc controls. Three community-scale activities follow. The first is honest benchmarking—every POSS-modified device should be compared with the strongest available non-POSS reference of the same class, prepared on the same substrate, in the same laboratory. The second

is data sharing in machine-readable form: structure–property–device datasets pooled across groups would train ML surrogates that no individual laboratory can produce alone. The third is targeted qualification work with foundries, roll-to-roll manufacturers, and packaging houses, transitioning POSS ILDs, encapsulants, and passivation layers from laboratory demonstrations into standardised product specifications. The chemistry of the POSS cage is well established; the coming decade will determine whether it can meet the requirements of manufacturing.

Author Contributions: Conceptualization, R.K. and M.U.; methodology, R.K.; investigation and literature curation, R.K., C.P. and N.S.; writing—original draft preparation, R.K., C.P. and N.S.; writing—review and editing, R.K. and M.U.; visualization, R.K., C.P. and N.S.; supervision, M.U.; project administration, R.K. All authors have read and agreed to the published version of the manuscript.

Funding: This research received no external funding.

Data Availability Statement: No new data were created or analyzed in this study. Data sharing is not applicable to this article.

Acknowledgments: The authors thank colleagues at Walailak University, Mahidol University, and Gunma University for helpful discussions. The authors used ChatGPT (GPT-4o) for language editing and formatting of the manuscript text. The device illustrations in the graphical abstract were generated with the generative AI image tool in Canva (Magic Media; web-based version; Canva Pty Ltd., Sydney, Australia) and subsequently edited by the authors.

Conflicts of Interest: The authors declare no conflicts of interest.

Abbreviations

The following abbreviations are used in this manuscript:

2D	two-dimensional
ACQ	aggregation-caused quenching
AI	artificial intelligence
AIBN	azobisisobutyronitrile
ALD	atomic layer deposition
ASTM	American Society for Testing and Materials
[BMIM][NTf_2]	1-butyl-3-methylimidazolium bis(trifluoromethanesulfonyl)imide
BEOL	back-end-of-line
BET	Brunauer–Emmett–Teller (surface area)
BODIPY	boron-dipyrromethene
CCT	correlated colour temperature
CIE	Commission Internationale de l'Éclairage (chromaticity coordinates)
CMP	chemical-mechanical polishing
C_{ox}	gate-dielectric capacitance per unit area
CRI	colour rendering index
CTE	coefficient of thermal expansion
CuAAC	copper-catalysed azide–alkyne cycloaddition
DDSQ	double-decker silsesquioxane
DFT	density functional theory
DMPA	2,2-dimethoxy-2-phenylacetophenone
DSSC	dye-sensitised solar cell
ECHA	European Chemicals Agency
EQE	external quantum efficiency
EUV	extreme ultraviolet
FAPA-MS	flowing-atmospheric-pressure-afterglow mass spectrometry
FF	fill factor
F-POSS	fluorinated polyhedral oligomeric silsesquioxane
GPC	gel permeation chromatography
HSQ	hydrogen silsesquioxane
HTL	hole-transport layer
IEC	International Electrotechnical Commission

IGZO	indium gallium zinc oxide
IL	ionic liquid
I_{on}/I_{off}	on/off current ratio
ILD	interlayer dielectric
IRDS	International Roadmap for Devices and Systems
ISO	International Organization for Standardization
ISOS	International Summit on Organic Photovoltaic Stability
ITRS	International Technology Roadmap for Semiconductors
JEDEC	Joint Electron Device Engineering Council
J_{sc}	short-circuit current density
K_{SV}	Stern–Volmer quenching constant
LED	light-emitting diode
LOD	limit of detection
LPSQ	ladder polysilsesquioxane
MCPA	2-methyl-4-chlorophenoxyacetic acid
ML	machine learning
MSQ	methylsilsesquioxane
NIR	near-infrared
NMR	nuclear magnetic resonance
OECD	Organisation for Economic Co-operation and Development
OFET	organic field-effect transistor
OLED	organic light-emitting diode
OPV	organic photovoltaic
OSC	organic solar cell
OVS	octavinylsilsesquioxane
P3HT	poly(3-hexylthiophene)
PBA	phenylbutylammonium
PCBM	[6,6]-phenyl-C_{61}-butyric acid methyl ester
PCE	power-conversion efficiency
PEA	phenethylammonium
PeLED	perovskite light-emitting diode
PEO	poly(ethylene oxide)
PFAS	per- and polyfluoroalkyl substances
PhOLED	phosphorescent organic light-emitting diode
PI	polyimide
PLQY	photoluminescence quantum yield
PMSQ	polymethylsilsesquioxane
PMSQ-CN	cyano-functionalised polymethylsilsesquioxane
POSS	polyhedral oligomeric silsesquioxane
PPMSQ	poly(phenyl-co-methacryl silsesquioxane)
PSC	perovskite solar cell
PU	polyurethane
PV	photovoltaic
PVA	poly(vinyl alcohol)
QDEF	quantum-dot enhancement film
QLED	quantum-dot light-emitting diode
QY	quantum yield
RAFT	reversible addition-fragmentation chain-transfer polymerisation
RH	relative humidity
RI	refractive index
ROMP	ring-opening metathesis polymerisation
RRAM	resistive random-access memory
rt	room temperature
SEM	scanning electron microscopy
SiCOH	carbon-doped silicon oxide (hydrogenated silicon oxycarbide)
SQ	silsesquioxane
St-POSS-SH	styrene-modified mercaptopropyl-polysilsesquioxane
TADF	thermally activated delayed fluorescence
$T_{d5\%}$	temperature at 5% mass loss (thermogravimetric analysis)
TDDB	time-dependent dielectric breakdown
T_g	glass-transition temperature

TIM	thermal interface material
T_{80}/T_{90}	time to 80%/90% of initial performance
T_n	polyhedral silsesquioxane cage with n silicon vertices (e.g., T_8, T_{10}, T_{12}, T_{14})
TTA	triplet–triplet annihilation
UV	ultraviolet
V_{oc}	open-circuit voltage
WLED	white light-emitting diode
WVTR	water-vapour transmission rate
XRD	X-ray diffraction
λ_{EL}	electroluminescence peak wavelength

References

1. Cordes, D.B.; Lickiss, P.D.; Rataboul, F. Recent Developments in the Chemistry of Cubic Polyhedral Oligosilsesquioxanes. *Chem. Rev.* **2010**, *110*, 2081–2173. [CrossRef] [PubMed]
2. Kausar, A. State-of-the-Art Overview on Polymer/POSS Nanocomposite. *Polym.-Plast. Technol. Eng.* **2017**, *56*, 1401–1420. [CrossRef]
3. Zhou, H.; Ye, Q.; Xu, J. Polyhedral oligomeric silsesquioxane-based hybrid materials and their applications. *Mater. Chem. Front.* **2017**, *1*, 212–230. [CrossRef]
4. Du, Y.; Liu, H. Cage-like silsesquioxanes-based hybrid materials. *Dalton Trans.* **2020**, *49*, 5396–5405. [CrossRef] [PubMed]
5. Moein, A.; Kebritchi, A. New Insights into the Structure, Properties, and Applications of Polyhedral Oligomeric Silsesquioxane. *Silicon* **2023**, *15*, 5845–5875. [CrossRef]
6. Wang, M.; Chi, H.; Joshy, K.S.; Wang, F. Progress in the Synthesis of Bifunctionalized Polyhedral Oligomeric Silsesquioxane. *Polymers* **2019**, *11*, 2098. [CrossRef] [PubMed]
7. Tunstall-Garcia, H.; Charles, B.L.; Evans, R.C. The Role of Polyhedral Oligomeric Silsesquioxanes in Optical Applications. *Adv. Photonics Res.* **2021**, *2*, 2000196. [CrossRef]
8. Li, Y.; Dong, X.-H.; Zou, Y.; Wang, Z.; Yue, K.; Huang, M.; Liu, H.; Feng, X.; Lin, Z.; Zhang, W.; et al. Polyhedral oligomeric silsesquioxane meets "click" chemistry: Rational design and facile preparation of functional hybrid materials. *Polymer* **2017**, *125*, 303–329. [CrossRef]
9. Laine, R.M.; Roll, M.F. Polyhedral Phenylsilsesquioxanes. *Macromolecules* **2011**, *44*, 1073–1109. [CrossRef]
10. Asuncion, M.Z.; Laine, R.M. Fluoride Rearrangement Reactions of Polyphenyl- and Polyvinylsilsesquioxanes as a Facile Route to Mixed Functional Phenyl, Vinyl T_{10} and T_{12} Silsesquioxanes. *J. Am. Chem. Soc.* **2010**, *132*, 3723–3736. [CrossRef] [PubMed]
11. Tanaka, K.; Chujo, Y. Advanced functional materials based on polyhedral oligomeric silsesquioxane (POSS). *J. Mater. Chem.* **2012**, *22*, 1733–1746. [CrossRef]
12. Sellinger, A.; Tamaki, R.; Laine, R.M.; Ueno, K.; Tanabe, H.; Williams, E.; Jabbour, G.E. Heck coupling of haloaromatics with octavinylsilsesquioxane: Solution processable nanocomposites for application in electroluminescent devices. *Chem. Commun.* **2005**, *41*, 3700–3702. [CrossRef] [PubMed]
13. Mohamed, M.G.; Kuo, S.W. Functional Polyimide/Polyhedral Oligomeric Silsesquioxane Nanocomposites. *Polymers* **2019**, *11*, 26. [CrossRef] [PubMed]
14. Grzelak, M.; Januszewski, R.; Marciniec, B. Synthesis and Hydrosilylation of Vinyl-Substituted Open-Cage Silsesquioxanes with Phenylsilanes: Regioselective Synthesis of Trifunctional Silsesquioxanes. *Inorg. Chem.* **2020**, *59*, 7830–7840. [CrossRef] [PubMed]
15. Mituła, K.; Duszczak, J.; Brząkalski, D.; Dudziec, B.; Kubicki, M.; Marciniec, B. Tetra-functional double-decker silsesquioxanes as anchors for reactive functional groups and potential synthons for hybrid materials. *Chem. Commun.* **2017**, *53*, 10370–10373. [CrossRef] [PubMed]
16. Huang, H.; Chen, B.; Wang, Z.; Hung, T.F.; Susha, A.S.; Zhong, H.; Rogach, A.L. Water resistant CsPbX3 nanocrystals coated with polyhedral oligomeric silsesquioxane and their use as solid state luminophores in all-perovskite white light-emitting devices. *Chem. Sci.* **2016**, *7*, 5699–5703. [CrossRef] [PubMed]
17. Kunthom, R.; Jaroentomeechai, T.; Ervithayasuporn, V. Polyhedral oligomeric silsesquioxane (POSS) containing sulfonic acid groups as a metal-free catalyst to prepare polycaprolactone. *Polymer* **2017**, *108*, 173–178. [CrossRef]
18. Kang, W.; An, G.; Kim, M.J.; Lee, W.H.; Lee, D.Y.; Kim, H.; Cho, J.H. Ladder-Type Silsesquioxane Copolymer Gate Dielectrics for High-Performance Organic Transistors and Inverters. *J. Phys. Chem. C* **2016**, *120*, 3501–3508. [CrossRef]
19. Yu, B.; Ha, Y.-G. Organic–inorganic hybrid gate dielectric using bifunctional polyhedral oligomeric silsesquioxane for low-voltage organic thin-film transistors. *Bull. Korean Chem. Soc.* **2021**, *42*, 1351–1356. [CrossRef]
20. Kim, M.J.; Heo, Y.M.; Cho, J.H. Ladder-type silsesquioxane copolymer gate dielectrics for gating solution-processed IGZO field-effect transistors. *Org. Electron.* **2017**, *43*, 41–46. [CrossRef]

21. Liu, B.-T.; Lin, H.-R.; Lee, R.-H.; Gorji, N.E.; Chou, J.-C. Fabrication and Characterization of an Efficient Inverted Perovskite Solar Cells with POSS Passivating Hole Transport Layer. *Nanomaterials* **2021**, *11*, 974. [CrossRef] [PubMed]
22. Kowalewska, A.; Majewska-Smolarek, K. Hybrid Perovskite-Based Materials Modified with Polyhedral Silsesquioxanes—Structure and Properties. *Materials* **2023**, *16*, 6531. [CrossRef] [PubMed]
23. Guan, P.; Wu, S.; Meng, H.; Li, Z.; Liu, M.; An, Y.; Liu, Y.; Xu, S.; Cao, S. Outstanding Stability and Resistive Switching Performance through Octa-Amino-Polyhedral Oligomeric Silsesquioxane Modification in Flexible Perovskite Resistive Random-Access Memories. *ACS Appl. Mater. Interfaces* **2024**, *16*, 66239–66249. [CrossRef] [PubMed]
24. Ding, S.; Zhao, S.; Gan, X.; Sun, A.; Xia, Y.; Liu, Y. Design of Fluorescent Hybrid Materials Based on POSS for Sensing Applications. *Molecules* **2022**, *27*, 3137. [CrossRef] [PubMed]
25. Ayandele, E.; Sarkar, B.; Alexandridis, P. Polyhedral Oligomeric Silsesquioxane (POSS)-Containing Polymer Nanocomposites. *Nanomaterials* **2012**, *2*, 445–475. [CrossRef] [PubMed]
26. Kim, J.; Park, Y.; Kwon, M.S. Recent progress in ladder-like polysilsesquioxane: Synthesis and applications. *Mater. Chem. Front.* **2024**, *8*, 2689–2726. [CrossRef]
27. Hunsicker, M.; Ankur; Morgenstern, B.; Zimmer, M.; Scheschkewitz, D. Polyhedral Oligomeric Silsesquioxane D_{3h}-$(RSiO_{1.5})_{14}$. *Chem. Eur. J.* **2024**, *30*, e202303640. [CrossRef] [PubMed]
28. Władyczyn, A.; John, Ł. Silsesquioxane Cages under Solvent Regimen: The Influence of the Solvent on the Hydrolysis and Condensation of Alkoxysilane. *Inorg. Chem.* **2024**, *63*, 9145–9155. [CrossRef] [PubMed]
29. Yoshida, K.; Hattori, T.; Ootake, N.; Tanaka, R.; Matsumoto, H. Silsesquioxane-Based Polymers: Synthesis of Phenylsilsesquioxanes with Double-Decker Structure and Their Polymers. In *Silicon Based Polymers: Advances in Synthesis and Supramolecular Organization*; Ganachaud, F., Boileau, S., Boury, B., Eds.; Springer: Dordrecht, The Netherlands, 2008; pp. 205–211. [CrossRef]
30. John, Ł.; Ejfler, J. A Brief Review on Selected Applications of Hybrid Materials Based on Functionalized Cage-like Silsesquioxanes. *Polymers* **2023**, *15*, 1452. [CrossRef] [PubMed]
31. Tanaka, T.; Hasegawa, Y.; Kawamori, T.; Kunthom, R.; Takeda, N.; Unno, M. Synthesis of Double-Decker Silsesquioxanes from Substituted Difluorosilane. *Organometallics* **2019**, *38*, 743–747. [CrossRef]
32. Kunthom, R.; Adachi, T.; Liu, Y.; Takeda, N.; Unno, M.; Tanaka, R. Synthesis of a "Butterfly Cage" Based on a Double-Decker Silsesquioxane. *Chem. Asian J.* **2019**, *14*, 4179–4182. [CrossRef] [PubMed]
33. Kunthom, R.; Takeda, N.; Unno, M. Synthesis and Characterization of Unsymmetrical Double-Decker Siloxane (Basket Cage). *Molecules* **2019**, *24*, 4252. [CrossRef] [PubMed]
34. Chaiprasert, T.; Liu, Y.; Intaraprecha, P.-K.; Kunthom, R.; Takeda, N.; Unno, M. Synthesis of Tricyclic Laddersiloxane with Various Ring Sizes (Bat Siloxane). *Macromol. Rapid Commun.* **2021**, *42*, 2000608. [CrossRef] [PubMed]
35. Liu, Y.; Takeda, N.; Ouali, A.; Unno, M. Synthesis, Characterization, and Functionalization of Tetrafunctional Double-Decker Siloxanes. *Inorg. Chem.* **2019**, *58*, 4093–4098. [CrossRef] [PubMed]
36. Oguri, N.; Egawa, Y.; Takeda, N.; Unno, M. Janus-Cube Octasilsesquioxane: Facile Synthesis and Structure Elucidation. *Angew. Chem. Int. Ed.* **2016**, *55*, 9336–9339. [CrossRef] [PubMed]
37. Blázquez-Moraleja, A.; Pérez-Ojeda, M.E.; Suárez, J.R.; Jimeno, M.L.; Chiara, J.L. Efficient multi-click approach to well-defined two-faced octasilsesquioxanes: The first perfect Janus nanocube. *Chem. Commun.* **2016**, *52*, 5792–5795. [CrossRef] [PubMed]
38. Duszczak-Kaczmarek, J.; Mituła-Chmielowiec, K.; Rzonsowska, M.; Jankowski, W.; Hoffmann, M.; Walkowiak, J.; Dudziec, B. Preparation of T_8 and double-decker silsesquioxane-based Janus-type molecules: Molecular modeling and DFT insights. *Sci. Rep.* **2024**, *14*, 18527. [CrossRef] [PubMed]
39. Hong, N.; Zhang, Y.; Sun, Q.; Fan, W.; Li, M.; Xie, M.; Fu, W. The Evolution of Organosilicon Precursors for Low-k Interlayer Dielectric Fabrication Driven by Integration Challenges. *Materials* **2021**, *14*, 4827. [CrossRef] [PubMed]
40. Zhang, W.; Camino, G.; Yang, R. Polymer/polyhedral oligomeric silsesquioxane (POSS) nanocomposites: An overview of fire retardance. *Prog. Polym. Sci.* **2017**, *67*, 77–125. [CrossRef]
41. Pielichowski, K.; Njuguna, J.; Janowski, B.; Pielichowski, J. Polyhedral Oligomeric Silsesquioxanes (POSS)-Containing Nanohybrid Polymers. In *Supramolecular Polymers Polymeric Betains Oligomers; Advances in Polymer Science*; Springer: Berlin/Heidelberg, Germany, 2006; Volume 201, pp. 225–296. [CrossRef]
42. Hao, L.; Chen, J.; Ma, T.; Cheng, J.; Zhang, J.; Zhao, F. Low dielectric and high performance of epoxy polymer via grafting POSS dangling chains. *Eur. Polym. J.* **2022**, *173*, 111313. [CrossRef]
43. Xie, M.; Li, G.; Fan, W.; Li, M.; Sun, Q.; Guo, J.; Xia, S.; Fu, W. Low dielectric silsesquioxane-modified benzocyclobutene composites. *Polymer* **2023**, *282*, 126188. [CrossRef]
44. Endo, H.; Takeda, N.; Takanashi, M.; Imai, T.; Unno, M. Refractive Indices of Silsesquioxanes with Various Structures. *Silicon* **2015**, *7*, 127–132. [CrossRef]
45. Koh, K.; Sohn, H. Fast Curable Polysiloxane-Silphenylene Hybrimer with High Transparency and Refractive Index for Optical Applications. *Polymers* **2021**, *13*, 515. [CrossRef] [PubMed]

46. Mabry, J.M.; Vij, A.; Iacono, S.T.; Viers, B.D. Fluorinated Polyhedral Oligomeric Silsesquioxanes (F-POSS). *Angew. Chem. Int. Ed.* **2008**, *47*, 4137–4140. [CrossRef] [PubMed]
47. Liu, N.; Du, Q.; Yin, G.; Liu, P.; Li, L.; Xie, H.; Zhu, C.; Li, Y.; Zhou, H.; Zhang, W.-B.; et al. Extremely low trap-state energy level perovskite solar cells passivated using NH_2-POSS with improved efficiency and stability. *J. Mater. Chem. A* **2018**, *6*, 6806–6814. [CrossRef]
48. Koymeth, S.; Paluch, M.; Dulski, M.; Wojnarowska, Z. Tuning Ionic Liquids with Charged Polyhedral Oligomeric Silsesquioxane Nanoparticles for Highly Conductive Quasi-Solid Electrolytes. *Nano Lett.* **2025**, *25*, 9779–9786. [CrossRef] [PubMed]
49. Wang, Y.; Liu, F.; Xue, X. Morphology and properties of UV-curing epoxy acrylate coatings modified with methacryl-POSS. *Prog. Org. Coat.* **2015**, *78*, 404–410. [CrossRef]
50. Pang, Z.; Sun, H.; Guo, Y.; Du, J.; Li, L.; Li, Q.; Yang, J.; Zhang, J.; Wu, W.; Yang, S. Research Advances of Porous Polyimide-Based Composites with Low Dielectric Constant. *Polymers* **2023**, *15*, 3341. [CrossRef] [PubMed]
51. Santiago-Portillo, A.; Cinà, V.; Carbonell, E.; Fusaro, L.; Lemaur, V.; Lazzaroni, R.; Gruttadauria, M.; Giacalone, F.; Aprile, C. White light emitting silsesquioxane based materials: The importance of a ligand with rigid and directional arms. *Mater. Adv.* **2022**, *3*, 570–578. [CrossRef]
52. Félix, G.; Sene, S.; Kulakova, A.; Bilyachenko, A.N.; Khrustalev, V.N.; Shubina, E.S.; Guari, Y.; Larionova, J. Tetranuclear lanthanide-based silsesquioxanes: Towards a combination of a slow relaxation of the magnetization and a luminescent thermometry. *RSC Adv.* **2023**, *13*, 26302–26312. [CrossRef] [PubMed]
53. Kaźmierczak, J.; Kuciński, K.; Hreczycho, G. Highly Efficient Catalytic Route for the Synthesis of Functionalized Silsesquioxanes. *Inorg. Chem.* **2017**, *56*, 9337–9342. [CrossRef] [PubMed]
54. Yu, T.; Xu, Z.; Su, W.; Zhao, Y.; Zhang, H.; Bao, Y. Highly efficient phosphorescent materials based on Ir(III) complexes-grafted on a polyhedral oligomeric silsesquioxane core. *Dalton Trans.* **2016**, *45*, 13491–13502. [CrossRef] [PubMed]
55. Yang, X.; Froehlich, J.D.; Chae, H.S.; Harding, B.T.; Li, S.; Mochizuki, A.; Jabbour, G.E. Efficient Light-Emitting Devices Based on Platinum-Complexes-Anchored Polyhedral Oligomeric Silsesquioxane Materials. *Chem. Mater.* **2010**, *22*, 4776–4782. [CrossRef]
56. Ye, Q.; Zhou, H.; Xu, J. Cubic Polyhedral Oligomeric Silsesquioxane Based Functional Materials: Synthesis, Assembly, and Applications. *Chem. Asian J.* **2016**, *11*, 1322–1337. [CrossRef] [PubMed]
57. Wang, Q.; Unno, M.; Liu, H. Silsesquioxane-Based Triphenylamine-Linked Fluorescent Porous Polymer for Dyes Adsorption and Nitro-Aromatics Detection. *Materials* **2021**, *14*, 3851. [CrossRef] [PubMed]
58. Gou, Z.; Zhang, X.; Zuo, Y.; Tian, M.; Dong, B.; Tang, Y.; Lin, W. Triphenylamine-based silsesquioxane derivatives for multiple anion recognition via anion effect and solvent effect. *Sens. Actuators B Chem.* **2021**, *338*, 129837. [CrossRef]
59. Čolović, M.; Volavšek, J.; Stathatos, E.; Čelan Korošin, N.; Šobak, M.; Jerman, I. Amphiphilic POSS-based ionic liquid electrolyte additives as a boost for dye-sensitized solar cell performance. *Sol. Energy* **2019**, *183*, 619–631. [CrossRef]
60. Żak, P.; Pietraszuk, C. Application of olefin metathesis in the synthesis of functionalized polyhedral oligomeric silsesquioxanes (POSS) and POSS-containing polymeric materials. *Beilstein J. Org. Chem.* **2019**, *15*, 310–332. [CrossRef] [PubMed]
61. Yamada, N.; Gon, M.; Tanaka, K. Synthesis of Full Color Hybrid Materials Using POSS Ionic Liquids. *Macromol. Rapid Commun.* **2026**, *47*, e00391. [CrossRef] [PubMed]
62. Lo, M.Y.; Zhen, C.; Lauters, M.; Jabbour, G.E.; Sellinger, A. Organic-Inorganic Hybrids Based on Pyrene Functionalized Octavinylsilsesquioxane Cores for Application in OLEDs. *J. Am. Chem. Soc.* **2007**, *129*, 5808–5809. [CrossRef] [PubMed]
63. Lin, M.; Luo, C.; Xing, G.; Chen, L.; Ling, Q. Influence of polyhedral oligomeric silsesquioxanes (POSS) on the luminescence properties of non-conjugated copolymers based on iridium complex and carbazole units. *RSC Adv.* **2017**, *7*, 39512–39522. [CrossRef]
64. Akhtar, P.; Mahato, R.; Singh Anand, T.; Hamrah, A.; Kumar Hazra, C.; Singh, M. Solution Processable Organic–Inorganic Hybrid POSS-MFPy as a Blue Emitter in OLEDs. *ACS Appl. Opt. Mater.* **2026**, *4*, 180–189. [CrossRef]
65. Chen, Z.; Feng, S.; Wang, D. Organosilicon Fluorescent Materials. *Polymers* **2023**, *15*, 332. [CrossRef] [PubMed]
66. Hsieh, Y.-T.; Lin, Y.-F.; Liu, W.-R. Enhancing the Water Resistance and Stability of $CsPbBr_3$ Perovskite Quantum Dots for Light-Emitting-Diode Applications through Encapsulation in Waterproof Polymethylsilsesquioxane Aerogels. *ACS Appl. Mater. Interfaces* **2020**, *12*, 58049–58059. [CrossRef] [PubMed]
67. Huang, H.; Lin, H.; Kershaw, S.V.; Susha, A.S.; Choy, W.C.H.; Rogach, A.L. Polyhedral Oligomeric Silsesquioxane Enhances the Brightness of Perovskite Nanocrystal-Based Green Light-Emitting Devices. *J. Phys. Chem. Lett.* **2016**, *7*, 4398–4404. [CrossRef] [PubMed]
68. Kim, J.S.; Heo, J.-M.; Park, G.-S.; Woo, S.-J.; Cho, C.; Yun, H.J.; Kim, D.-H.; Park, J.; Lee, S.-C.; Park, S.-H.; et al. Ultra-bright, efficient and stable perovskite light-emitting diodes. *Nature* **2022**, *611*, 688–694. [CrossRef] [PubMed]
69. Bai, W.; Xuan, T.; Zhao, H.; Dong, H.; Cheng, X.; Wang, L.; Xie, R.-J. Perovskite Light-Emitting Diodes with an External Quantum Efficiency Exceeding 30%. *Adv. Mater.* **2023**, *35*, 2302283. [CrossRef] [PubMed]
70. Wang, Y.; Vaneski, A.; Yang, H.; Gupta, S.; Hetsch, F.; Kershaw, S.V.; Teoh, W.Y.; Li, H.; Rogach, A.L. Polyhedral Oligomeric Silsesquioxane as a Ligand for CdSe Quantum Dots. *J. Phys. Chem. C* **2013**, *117*, 1857–1862. [CrossRef]

71. Huo, Q.; Lv, Z.; Feng, S.; Wang, D.; Liu, H. Tuning White-Light Emission of POSS-Based Fluorescent Hybrid Porous Polymers via Physical Blending for White LEDs. *Polymers* **2025**, *17*, 2558. [CrossRef] [PubMed]
72. Gan, Y.; Jiang, X.; Yin, J. Thiol–ene photo-curable hybrid silicone resin for LED encapsulation: Enhancement of light extraction efficiency by facile self-keeping hemisphere coating. *J. Mater. Chem. C* **2014**, *2*, 5533–5539. [CrossRef]
73. Wu, J.; Fei, F.; Wei, C.; Chen, X.; Nie, S.; Zhang, D.; Su, W.; Cui, Z. Efficient multi-barrier thin film encapsulation of OLED using alternating Al_2O_3 and polymer layers. *RSC Adv.* **2018**, *8*, 5721–5727. [CrossRef] [PubMed]
74. Shi, K.; Wu, C.; Zhang, H.; Tong, K.-N.; He, W.; Li, W.; Jin, Z.; Jung, S.; Li, S.; Wang, X.; et al. Enhanced Emitting Dipole Orientation Based on Asymmetric Iridium(III) Complexes for Efficient Saturated-Blue Phosphorescent OLEDs. *Adv. Sci.* **2024**, *11*, 2402349. [CrossRef] [PubMed]
75. Afolayan, E.O.; Dursun, I.; Pizano, A.; Lang, C.; Lungwitz, D.; Kondakova, M.; Boroson, M.; Kahn, A.; Hickner, M.; Giebink, N.C. Improved Light Extraction in Organic Light-Emitting Diodes via Semiconductor Dilution. *Adv. Opt. Mater.* **2024**, *12*, 2302588. [CrossRef]
76. Panfil, Y.E.; Oded, M.; Banin, U. Colloidal Quantum Nanostructures: Emerging Materials for Display Applications. *Angew. Chem. Int. Ed.* **2018**, *57*, 4274–4295. [CrossRef] [PubMed]
77. Hu, H.; Levchuk, I.; Kalkowski, F.; Elia, J.; Osvet, A.; Brabec, C.J. Engineering Stable Perovskite Film for High Color Purity Display Application. *ACS Energy Lett.* **2023**, *8*, 4380–4385. [CrossRef]
78. Mannodi-Kanakkithodi, A.; Park, J.-S.; Martinson, A.B.F.; Chan, M.K.Y. Defect Energetics in Pseudo-Cubic Mixed Halide Lead Perovskites from First-Principles. *J. Phys. Chem. C* **2020**, *124*, 16729–16738. [CrossRef]
79. Zheng, X.; Yuan, S.; Liu, J.; Yin, J.; Yuan, F.; Shen, W.-S.; Yao, K.; Wei, M.; Zhou, C.; Song, K.; et al. Chlorine Vacancy Passivation in Mixed Halide Perovskite Quantum Dots by Organic Pseudohalides Enables Efficient Rec. 2020 Blue Light-Emitting Diodes. *ACS Energy Lett.* **2020**, *5*, 793–798. [CrossRef]
80. Zhang, K.; Shen, Y.; Cao, L.-X.; Su, Z.-H.; Hu, X.-M.; Feng, S.-C.; Wang, B.-F.; Xie, F.-M.; Li, H.-Z.; Gao, X.; et al. Nondestructive halide exchange via SN2-like mechanism for efficient blue perovskite light-emitting diodes. *Nat. Commun.* **2024**, *15*, 10621. [CrossRef] [PubMed]
81. Matsukawa, K.; Watanabe, M.; Hamada, T.; Nagase, T.; Naito, H. Polysilsesquioxanes for Gate-Insulating Materials of Organic Thin-Film Transistors. *Int. J. Polym. Sci.* **2012**, *2012*, 852063. [CrossRef]
82. Wang, J.; Sun, J.; Zhou, J.; Jin, K.; Fang, Q. Fluorinated and Thermo-Cross-Linked Polyhedral Oligomeric Silsesquioxanes: New Organic–Inorganic Hybrid Materials for High-Performance Dielectric Application. *ACS Appl. Mater. Interfaces* **2017**, *9*, 12782–12790. [CrossRef] [PubMed]
83. Liu, X.; Zhou, J.; Zhou, Y.; Wu, M.; Zhu, Y.; Zhao, J.; Liu, S.; Xiao, H. Chemically crosslinked polyimide-POSS hybrid: A dielectric material with improved dimensional stability and dielectric properties. *Eur. Polym. J.* **2022**, *173*, 111315. [CrossRef]
84. Lee, Y.-J.; Huang, J.-M.; Kuo, S.-W.; Lu, J.-S.; Chang, F.-C. Polyimide and polyhedral oligomeric silsesquioxane nanocomposites for low-dielectric applications. *Polymer* **2005**, *46*, 173–181. [CrossRef]
85. Leu, C.-M.; Chang, Y.-T.; Wei, K.-H. Polyimide-Side-Chain Tethered Polyhedral Oligomeric Silsesquioxane Nanocomposites for Low-Dielectric Film Applications. *Chem. Mater.* **2003**, *15*, 3721–3727. [CrossRef]
86. Liu, Y.; Zhao, J.-Q.; Sun, W.-J.; Huang, Y.-K.; Chen, S.-J.; Guo, X.-J.; Zhang, Q. A Facile Photo-cross-linking Method for Polymer Gate Dielectrics and Their Applications in Fully Solution Processed Low Voltage Organic Field-effect Transistors on Plastic Substrate. *Chin. J. Polym. Sci.* **2018**, *36*, 918–924. [CrossRef]
87. Hwang, D.-H.; Yang, Y.S.; Lee, J.-I.; Kim, S.H.; Park, O.-H.; Kim, H.-C.; Lee, V.; Dubois, G.; Miller, R.D. Organic thin film transistor using a photo-curable organic/inorganic hybrid material as a gate dielectric. *J. Nanosci. Nanotechnol.* **2008**, *8*, 4561–4564. [CrossRef] [PubMed]
88. Ng, W.H.; Mehonic, A.; Buckwell, M.; Montesi, L.; Kenyon, A.J. High-Performance Resistance Switching Memory Devices Using Spin-On Silicon Oxide. *IEEE Trans. Nanotechnol.* **2018**, *17*, 884–888. [CrossRef]
89. Grill, A.; Gates, S.M.; Ryan, T.E.; Nguyen, S.V.; Priyadarshini, D. Progress in the development and understanding of advanced low k and ultralow k dielectrics for very large-scale integration interconnects—State of the art. *Appl. Phys. Rev.* **2014**, *1*, 011306. [CrossRef]
90. Sa, Y.K.; Bang, J.; Son, J.; Yu, D.-Y.; Kim, Y.-C. Enhanced Thermo-Mechanical Reliability of Ultralow-K Dielectrics with Self-Organized Molecular Pores. *Materials* **2021**, *14*, 2284. [CrossRef] [PubMed]
91. Wu, Q.; Bhattacharya, M.; Moore, L.M.J.; Morgan, S.E. POSS-enhanced phase separation in air-processed P3HT:PCBM bulk heterojunction photovoltaic systems. *ACS Appl. Mater. Interfaces* **2013**, *5*, 6136–6146. [CrossRef] [PubMed]
92. Rathnayake, H.; White, J.; Dawood, S. Polysilsesquioxane-based organic-inorganic hybrid nanomaterials and their applications towards organic photovoltaics. *Synth. Met.* **2021**, *273*, 116705. [CrossRef]
93. Song, H.; Hu, D.; Lv, J.; Lu, S.; Haiyan, C.; Kan, Z. Hybrid Cathode Interlayer Enables 17.4% Efficiency Binary Organic Solar Cells. *Adv. Sci.* **2022**, *9*, 2105575. [CrossRef] [PubMed]

94. Chen, C.; Wang, L.; Xiao, W.; Qian, Y.; Jiao, Y.; Liu, S.; Meng, X.; Ma, W.; Li, Y.; Li, Y. Organic solar cells with 20.82% efficiency and high tolerance of active layer thickness through crystallization sequence manipulation. *Nat. Mater.* **2025**, *24*, 444–453. [CrossRef] [PubMed]
95. Zhou, J.; Liu, Z.; Yu, P.; Tong, G.; Chen, R.; Ono, L.K.; Chen, R.; Wang, H.; Ren, F.; Liu, S.; et al. Modulation of perovskite degradation with multiple-barrier for light-heat stable perovskite solar cells. *Nat. Commun.* **2023**, *14*, 6120. [CrossRef] [PubMed]
96. Liang, H.; Wu, F.; Xia, R.; Wu, W.; Li, S.; Di, P.; Yang, M. In-situ synthesized perovskite/polyhedral oligomeric silsesquioxane nanocomposites for robust X-ray imaging. *iScience* **2024**, *27*, 110951. [CrossRef] [PubMed]
97. Kakiage, K.; Aoyama, Y.; Yano, T.; Otsuka, T.; Kyomen, T.; Unno, M.; Hanaya, M. An achievement of over 12 percent efficiency in an organic dye-sensitized solar cell. *Chem. Commun.* **2014**, *50*, 6379–6381. [CrossRef] [PubMed]
98. National Renewable Energy Laboratory. *Best Research-Cell Efficiency Chart*; NREL: Golden, CO, USA, 2026. Available online: https://www.nrel.gov/pv/cell-efficiency (accessed on 2 September 2026).
99. Cao, M.; Ji, W.; Chao, C.; Li, J.; Dai, F.; Fan, X. Recent Advances in UV-Cured Encapsulation for Stable and Durable Perovskite Solar Cell Devices. *Polymers* **2023**, *15*, 3911. [CrossRef] [PubMed]
100. Li, W.; Feng, S. New Functionalized Ionic Liquids Based on POSS for the Detection of Fe^{3+} Ion. *Polymers* **2021**, *13*, 196. [CrossRef] [PubMed]
101. Liu, H.; Chen, Z.; Feng, S.; Wang, D.; Liu, H. A Selenone-Functionalized Polyhedral Oligomeric Silsesquioxane for Selective Detection and Adsorption of Hg^{2+} ions in Aqueous Solutions. *Polymers* **2019**, *11*, 2084. [CrossRef] [PubMed]
102. Dare, E.O.; Akinhanmi, T.F.; Aremu, J.A.; Adetunji, O.R.; Bamgbose, J.T.; Vendrell-Criado, V.; Jiménez, M.C.; Pérez-Ruiz, R.; Bonardd, S.; Díaz Díaz, D. Dual-mode colorimetric/fluorescent chemosensor for Cu^{2+}/Zn^{2+} and fingerprint imaging based on rhodamine ethylenediamine bis(triazolyl silsesquioxane). *Photochem. Photobiol. Sci.* **2023**, *22*, 1527–1541. [CrossRef] [PubMed]
103. Wang, D.; Li, L.; Yang, W.; Zuo, Y.; Feng, S.; Liu, H. POSS-based luminescent porous polymers for carbon dioxide sorption and nitroaromatic explosives detection. *RSC Adv.* **2014**, *4*, 59877–59884. [CrossRef]
104. Wang, Z.; Kunthom, R.; Kostjuk, S.V.; Liu, H. Near-infrared-emitting silsesquioxane-based porous polymer containing thiophene for highly efficient adsorption and detection of iodine vapor and solution phase. *Eur. Polym. J.* **2023**, *192*, 112072. [CrossRef]
105. He, H.-B.; Dong, C.; Li, B.; Dong, J.-P.; Bo, T.-Y.; Wang, T.-L.; Yu, Q.-W.; Feng, Y.-Q. Fabrication of enrofloxacin imprinted organic–inorganic hybrid mesoporous sorbent from nanomagnetic polyhedral oligomeric silsesquioxanes for the selective extraction of fluoroquinolones in milk samples. *J. Chromatogr. A* **2014**, *1361*, 23–33. [CrossRef] [PubMed]
106. He, H.; Wang, Y.; Zhou, Z.; Guo, Y.; Yan, X.; Lei, Y.; Shen, X.; Liu, W.; Luo, L. Boronate affinity directing adenosine imprinted nanomagnetic polyhedral oligomeric silsesquioxanes for selective extraction of nucleosides in urine sample. *Microchem. J.* **2021**, *169*, 106575. [CrossRef]
107. Zhao, H.; She, W.; Shi, D.; Wu, W.; Zhang, Q.-C.; Li, R.K.Y. Polyurethane/POSS nanocomposites for superior hydrophobicity and high ductility. *Compos. Part B Eng.* **2019**, *177*, 107441. [CrossRef]
108. Shao, L.; Li, Y.; Ma, Z.; Bai, Y.; Wang, J.; Zeng, P.; Gong, P.; Shi, F.; Ji, Z.; Qiao, Y.; et al. Highly Sensitive Strain Sensor Based on a Stretchable and Conductive Poly(vinyl alcohol)/Phytic Acid/NH_2-POSS Hydrogel with a 3D Microporous Structure. *ACS Appl. Mater. Interfaces* **2020**, *12*, 26496–26508. [CrossRef] [PubMed]
109. Chruściel, J.J. Self-Healing Silsesquioxane-Based Materials. *Polymers* **2022**, *14*, 1869. [CrossRef] [PubMed]
110. Behera, P.K.; Mondal, P.; Singha, N.K. Self-Healable and Ultrahydrophobic Polyurethane-POSS Hybrids by Diels-Alder "Click" Reaction: A New Class of Coating Material. *Macromolecules* **2018**, *51*, 4770–4781. [CrossRef]
111. Lin, C.-H.; Chen, W.-B.; Whang, W.-T.; Chen, C.-H. Characteristics of Thermosetting Polymer Nanocomposites: Siloxane-Imide-Containing Benzoxazine with Silsesquioxane Epoxy Resins. *Polymers* **2020**, *12*, 2510. [CrossRef] [PubMed]
112. Sun, X.; Wang, J.; Fu, Q.; Zhang, Q.; Xu, R. Synthesis of a Novel Bifunctional Epoxy Double-Decker Silsesquioxane: Improvement of the Thermal Stability and Dielectric Properties of Polybenzoxazine. *Polymers* **2022**, *14*, 5154. [CrossRef] [PubMed]
113. Kao, Y.C.; Chen, W.C.; El-Mahdy, A.F.M.; Hsu, M.Y.; Lin, C.H.; Kuo, S.W. High Thermal Resistance of Epoxy/Cyanate Ester Hybrids Incorporating an Inorganic Double-Decker-Shaped Polyhedral Silsesquioxane Nanomaterial. *Molecules* **2022**, *27*, 5938. [CrossRef] [PubMed]
114. Guadagno, L.; Sorrentino, A.; Longo, R.; Raimondo, M. Multifunctional Properties of Polyhedral Oligomeric Silsesquioxanes (POSS)-Based Epoxy Nanocomposites. *Polymers* **2023**, *15*, 2297. [CrossRef] [PubMed]
115. Zhang, M.; Liu, H. Silsesquioxane-Based Hybrid Semiconductor Polymers for Efficient Antibiotic Photodegradation and Detection Simultaneously. *ACS Appl. Polym. Mater.* **2025**, *7*, 4633–4643. [CrossRef]
116. Rzonsowska, M.; Lusina, A.; Dudziec, B.; Hoogenboom, R.; Cegłowski, M. Porous Silsesquioxane-Polyoxazoline Hybrid Materials for Adsorption and Quantification of Pesticides in Environmental Samples. *Chem. Mater.* **2026**, *38*, 3581–3595. [CrossRef]
117. Kato, K.; Gon, M.; Tanaka, K.; Chujo, Y. Stretchable Conductive Hybrid Films Consisting of Cubic Silsesquioxane-capped Polyurethane and Poly(3-hexylthiophene). *Polymers* **2019**, *11*, 1195. [CrossRef] [PubMed]

118. Zhao, L.; Yan, L.; Wei, C.; Li, Q.; Huang, X.; Wang, Z.; Fu, M.; Ren, J. Significantly Improve the Thermal Conductivity and Dielectric Performance of Epoxy Composite by Introducing Boron Nitride and POSS. *Nanomaterials* **2024**, *14*, 205. [CrossRef] [PubMed]
119. Guenthner, A.J.; Lamison, K.R.; Lubin, L.M.; Haddad, T.S.; Mabry, J.M. Hansen Solubility Parameters for Octahedral Oligomeric Silsesquioxanes. *Ind. Eng. Chem. Res.* **2012**, *51*, 12282–12293. [CrossRef]
120. Ullah, A.; Ullah, S.; Khan, G.S.; Shah, S.M.; Hussain, Z.; Muhammad, S.; Siddiq, M.; Hussain, H. Water soluble polyhedral oligomeric silsesquioxane based amphiphilic hybrid polymers: Synthesis, self-assembly, and applications. *Eur. Polym. J.* **2016**, *75*, 67–92. [CrossRef]
121. Mansfield, E.; Barnes, B.; Kline, R.J.; Vladar, A.E.; Obeng, Y.S.; Davydov, A. *International Roadmap for Devices and Systems (IRDS), 2023 Edition: Metrology*; IEEE: Piscataway, NJ, USA, 2023.
122. Wen, Z.; Liu, X.; Chen, W.; Zhou, R.; Wu, H.; Xia, Y.; Wu, L. Progress in Polyhedral Oligomeric Silsesquioxane (POSS) Photoresists: A Comprehensive Review across Lithographic Systems. *Polymers* **2024**, *16*, 846. [CrossRef] [PubMed]
123. Zhang, R.-S.; Miao, L.; Lu, X.-Y.; Li, Q.; Luo, F.; Qiu, H.-Y.; Wu, G.-P. Norbornene and Epoxide-Substituted Silsesquioxane Photoresists with High-Sensitivity and Stability. *ACS Nano* **2025**, *19*, 38243–38254. [CrossRef] [PubMed]
124. Rathore, A.; Pollentier, I.; Cipriani, M.; Singh, H.; De Simone, D.; Ingólfsson, O.; De Gendt, S. Extreme Ultraviolet-Printability and Mechanistic Studies of Engineered Hydrogen Silsesquioxane Photoresist Systems. *ACS Appl. Polym. Mater.* **2021**, *3*, 1964–1972. [CrossRef]
125. OECD. *Reconciling Terminology of the Universe of Per- and Polyfluoroalkyl Substances: Recommendations and Practical Guidance*; OECD Series on Risk Management of Chemicals, No. 61; ENV/CBC/MONO(2021)25; OECD Publishing: Paris, France, 2021. [CrossRef]
126. Danish Environmental Protection Agency; German Federal Institute for Occupational Safety and Health (BAuA); National Institute for Public Health and the Environment (RIVM), The Netherlands; Norwegian Environment Agency; Swedish Chemicals Agency (KEMI). *Annex XV Restriction Report: Proposal for a Restriction—Per- and Polyfluoroalkyl Substances (PFASs), Version 2*; European Chemicals Agency: Helsinki, Finland, 2023; Available online: https://echa.europa.eu/restrictions-under-consideration/-/substance-rev/72301/term. (accessed on 2 September 2026).
127. Ellinas, K.; Tserepi, A.; Gogolides, E. Durable superhydrophobic and superamphiphobic polymeric surfaces and their applications: A review. *Adv. Colloid Interface Sci.* **2017**, *250*, 132–157. [CrossRef] [PubMed]
128. Wang, Y.; Pan, R.; Zhang, J.; Qian, J.; Basset, J.-M.; Jérôme, F.; Mignani, G.; Sun, D.; Zhou, L. Fluorine-Free POSS-Based Silane Coatings for Robust Superhydrophobic and Self-Cleaning Cotton Fabrics With Efficient Oil-Water Separation Performance. *J. Appl. Polym. Sci.* **2026**, *143*, e58085. [CrossRef]
129. Sun, D.; Wang, W.; Yu, D. Highly hydrophobic cotton fabrics prepared with fluorine-free functionalized silsesquioxanes. *Cellulose* **2017**, *24*, 4519–4531. [CrossRef]
130. Lee, J.; Park, D.; Lee, M.; Lee, H.; Park, K.; Lee, I.; Ryu, S. Machine learning-based inverse design methods considering data characteristics and design space size in materials design and manufacturing: A review. *Mater. Horiz.* **2023**, *10*, 5436–5456. [CrossRef] [PubMed]
131. Coley, C.W.; Eyke, N.S.; Jensen, K.F. Autonomous Discovery in the Chemical Sciences Part I: Progress. *Angew. Chem. Int. Ed.* **2020**, *59*, 22858–22893. [CrossRef] [PubMed]
132. Ghanbari, H.; Cousins, B.G.; Seifalian, A.M. A Nanocage for Nanomedicine: Polyhedral Oligomeric Silsesquioxane (POSS). *Macromol. Rapid Commun.* **2011**, *32*, 1032–1046. [CrossRef] [PubMed]
133. Kang, S.-K.; Murphy, R.K.J.; Hwang, S.-W.; Lee, S.M.; Harburg, D.V.; Krueger, N.A.; Shin, J.; Gamble, P.; Cheng, H.; Yu, S.; et al. Bioresorbable silicon electronic sensors for the brain. *Nature* **2016**, *530*, 71–76. [CrossRef] [PubMed]
134. Kulakova, A.N.; Nigoghossian, K.; Félix, G.; Khrustalev, V.N.; Shubina, E.S.; Long, J.; Guari, Y.; Carlos, L.D.; Bilyachenko, A.N.; Larionova, J. New Magnetic and Luminescent Dy(III) and Dy(III)/Y(III) Based Tetranuclear Silsesquioxane Cages. *Eur. J. Inorg. Chem.* **2021**, *2021*, 2696–2701. [CrossRef]
135. Zeng, S.; Liu, C.; Zhou, P. Transistor engineering based on 2D materials in the post-silicon era. *Nat. Rev. Electr. Eng.* **2024**, *1*, 335–348. [CrossRef]
136. Xu, Y.; Liu, K.; Xiong, X.; Wu, Y.; Zhai, T. Towards state-of-the-art semiconductor/dielectric interface in two-dimensional electronics. *J. Mater. Sci. Technol.* **2025**, *239*, 93–108. [CrossRef]
137. Molaei, M.J.; Younas, M.; Rezakazemi, M. A Comprehensive Review on Recent Advances in Two-Dimensional (2D) Hexagonal Boron Nitride. *ACS Appl. Electron. Mater.* **2021**, *3*, 5165–5187. [CrossRef]
138. Reese, M.O.; Gevorgyan, S.A.; Jørgensen, M.; Bundgaard, E.; Kurtz, S.R.; Ginley, D.S.; Olson, D.C.; Lloyd, M.T.; Morvillo, P.; Katz, E.A.; et al. Consensus stability testing protocols for organic photovoltaic materials and devices. *Sol. Energy Mater. Sol. Cells* **2011**, *95*, 1253–1267. [CrossRef]
139. Khenkin, M.V.; Katz, E.A.; Abate, A.; Bardizza, G.; Berry, J.J.; Brabec, C.; Brunetti, F.; Bulović, V.; Burlingame, Q.; Di Carlo, A.; et al. Consensus statement for stability assessment and reporting for perovskite photovoltaics based on ISOS procedures. *Nat. Energy* **2020**, *5*, 35–49. [CrossRef]

140. *JESD22-A101D.01*; Steady-State Temperature-Humidity Bias Life Test. JEDEC Solid State Technology Association: Arlington, VA, USA, 2021.
141. *ASTM D3359-23*; Standard Test Methods for Rating Adhesion by Tape Test. ASTM International: West Conshohocken, PA, USA, 2023.
142. *ISO 4287:1997*; Geometrical Product Specifications (GPS)—Surface Texture: Profile Method—Terms, Definitions and Surface Texture Parameters. International Organization for Standardization: Geneva, Switzerland, 1997.
143. *IEC 62631-3-1:2023*; Dielectric and Resistive Properties of Solid Insulating Materials—Part 3-1: Determination of Resistive Properties (DC Methods)—Volume Resistance and Volume Resistivity—General Method. International Electrotechnical Commission: Geneva, Switzerland, 2023.
144. *IEC 62631-3-2:2023*; Dielectric and Resistive Properties of Solid Insulating Materials—Part 3-2: Determination of Resistive Properties (DC Methods)—Surface Resistance and Surface Resistivity. International Electrotechnical Commission: Geneva, Switzerland, 2023.
145. *IEC 60112:2025*; Method for the Determination of the Proof and the Comparative Tracking Indices of Solid Insulating Materials. International Electrotechnical Commission: Geneva, Switzerland, 2025.
146. *IEC 61215-1:2021*; Terrestrial Photovoltaic (PV) Modules—Design Qualification and Type Approval—Part 1: Test Requirements. International Electrotechnical Commission: Geneva, Switzerland, 2021.

Disclaimer/Publisher's Note: The statements, opinions and data contained in all publications are solely those of the individual author(s) and contributor(s) and not of MDPI and/or the editor(s). MDPI and/or the editor(s) disclaim responsibility for any injury to people or property resulting from any ideas, methods, instructions or products referred to in the content.